

Supplementary Information for

Efficient light-harvesting, energy migration, and charge transfer by nanographene-based nonfullerene acceptor small-molecule exhibiting unusually long excited-state lifetime in film state

Tomokazu Umeyama,^{*a} Kensho Igarashi,^a Daiki Sasada,^a Yasunari Tamai,^{bc} Keiichi Ishida,^a
Tomoyuki Koganezawa,^d Shunsuke Ohtani,^b Kazuo Tanaka,^b Hideo Ohkita^{*b}
and Hiroshi Imahori^{*ac}

^a *Department of Molecular Engineering, Graduate School of Engineering, Kyoto University, Nishikyo-ku, Kyoto, 615-8510, Japan*

^b *Department of Polymer Chemistry, Graduate School of Engineering, Kyoto University, Nishikyo-ku, Kyoto 615-8510, Japan*

^c *Japan Science and Technology Agency (JST), PRESTO, 4-1-8 Honcho Kawaguchi, Saitama 332-0012, Japan*

^d *Japan Synchrotron Radiation Research Institute, 1-1-1, Kouto, Sayo-cho, Sayo-gun, Hyogo 679-5198, Japan*

^e *Institute for Integrated Cell-Material Sciences (WPI-iCeMS), Kyoto University, Sakyo-ku, Kyoto 606-8501, Japan*

E-mail: umeyama@scl.kyoto-u.ac.jp, ohkita@photo.polym.kyoto-u.ac.jp, imahori@scl.kyoto-u.ac.jp

Experimental

Instruments. ^1H NMR and ^{13}C NMR spectra were measured with a JEOL JNM-EX400 NMR spectrometer. High-resolution mass spectra were measured on a Thermo Fisher Scientific EXACTIVE (APCI) and LTQ orbitrap XL (MALDI). Attenuated total reflectance (ATR) FT-IR spectra were recorded on a ThermoFisher Scientific Nicolet 6700 FT-IR. Dynamic light scattering (DLS) measurements were performed using a Horiba LB550 particle size analyzer. Thermogravimetric analysis (TGA) measurements were conducted with a SHIMADZU TG-60 under flowing nitrogen at a scan rate of $10\text{ }^\circ\text{C min}^{-1}$. Differential scanning calorimetry (DSC) analysis was made on a SHIMADZU DSC-60 at a scan rate of $5\text{ }^\circ\text{C min}^{-1}$. UV–vis–near infrared (NIR) absorption spectra were obtained on a Perkin Elmer Lambda 900UV/vis/NIR spectrometer. Steady-state fluorescence spectra were recorded on a HORIBA NanoLog spectrofluorometer. Cyclic voltammetry (CV) and differential pulse voltammetry (DPV) measurements were performed using an ALS 630A electrochemical analyzer in dichloromethane containing 0.1 M tetra-*n*-butylammonium hexafluorophosphate (Bu_4NPF_6) as a supporting electrolyte. Absolute photoluminescence quantum efficiencies were determined using a HAMAMATSU PHOTONICS Quantaaurus-QY Plus Absolute PL quantum yield spectrometer C13534-01. Time-correlated single photon counting (TCSPC) measurements using a HORIBA NanoLOG-TCSPC were conducted for fluorescence lifetime measurements on the nanosecond time-scale. The time resolution was ca. 200 ps. Atomic force microscopy (AFM) analyses were carried out with an Asylum Technology MFP-3D-SA in the AC mode.

Photocurrent-voltage characteristics were measured by Keithley 2400 SourceMeter under a nitrogen atmosphere and simulated solar light (100 mW cm^{-2} , AM1.5) with OTENTO-SUN III solar simulator (Bunkoukeiki). Photocurrent action spectra were recorded with CEP-2000RR (Bunkoukeiki). Current–voltage characteristics of the electron- and hole-only devices for space charge-limited current (SCLC) measurements were conducted using Keithley 2400 SourceMeter under a nitrogen atmosphere.

Theoretical calculations. Geometry optimization and electronic structure calculations were performed using density functional theory (DFT) at the RB3LYP/6-31G(d) level. Calculations were carried out using the Gaussian 09 program.^{S1} All structures were fully optimized without any symmetry restriction.

Fabrication of OPV device based on ITIC. OPV devices were prepared on patterned indium tin oxide (ITO) substrates which were cleaned by ultra-sonication in deionized water, CHCl₃, acetone, and tetramethyl-ammonium hydroxide aqueous solution for 15 min each, and then deionized water for 25 min, followed by 2-propanol and ethanol for 15 min each. They were subsequently dried under nitrogen flow, and treated in a UV–ozone cleaner for 25 min. A solution of Zn(OAc)₂·2H₂O (55 mg), 2-methoxyethanol (1 mL), ethanolamine (15.6 μL) was stirred at room temperature, and was spin-coated on substrates at 3000 rpm for 20 s. The ZnO layer was dried at 200 °C for 30 min, and then transferred into a glove box filled with dried N₂ gas to coat the active layer. A blend solution of PBDB-T with ITIC ([PBDB-T] = 9 mg mL⁻¹, [PBDB-T]:[ITIC] = 1:0.7, w/w) in chlorobenzene with 1,8-diiodooctane (0.5 vol.%) was prepared and stirred on a hotplate at 40 °C for 3 h. The active layer was spin-coated at 2000 rpm for 20 s on the top of the ZnO layer, and the samples were annealed at 100 °C for 10 min. The thicknesses of the photoactive layers were ca. 100 nm. All samples were finally transferred to an evaporation chamber for MoO₃ deposition (~10 nm) at a rate of 0.1–0.3 Å s⁻¹ and Ag deposition (~100 nm) at a rate of 1–2 Å s⁻¹ before extracting their *J–V* characteristics (under AM1.5 conditions). OPV devices had the architecture of ITO/ZnO/PBDB-T:ITIC/MoO₃/Ag.

SCLC measurements. The hole and electron mobilities were measured using the SCLC method by using devices with the configurations of ITO/PEDOT:PSS/PBDB-T:NFA/MoO₃/Au for hole and ITO/ZnO/NFA/Al or ITO/ZnO/PBDB-T:NFA/Al for electron by taking current–voltage curves and fitting the results to a space charge limited form, where the SCLC is described by:

$$J = 9\varepsilon_0\varepsilon_r\mu V^2/8L^3$$

where ϵ_0 is the permittivity of free space, ϵ_r is the dielectric constant of the polymer, μ is the charge mobility, V is the voltage drop across the device, and L is the thickness of the blend film. The dielectric constant ϵ_r is assumed to be 3, which is a typical value for organic semiconductors.

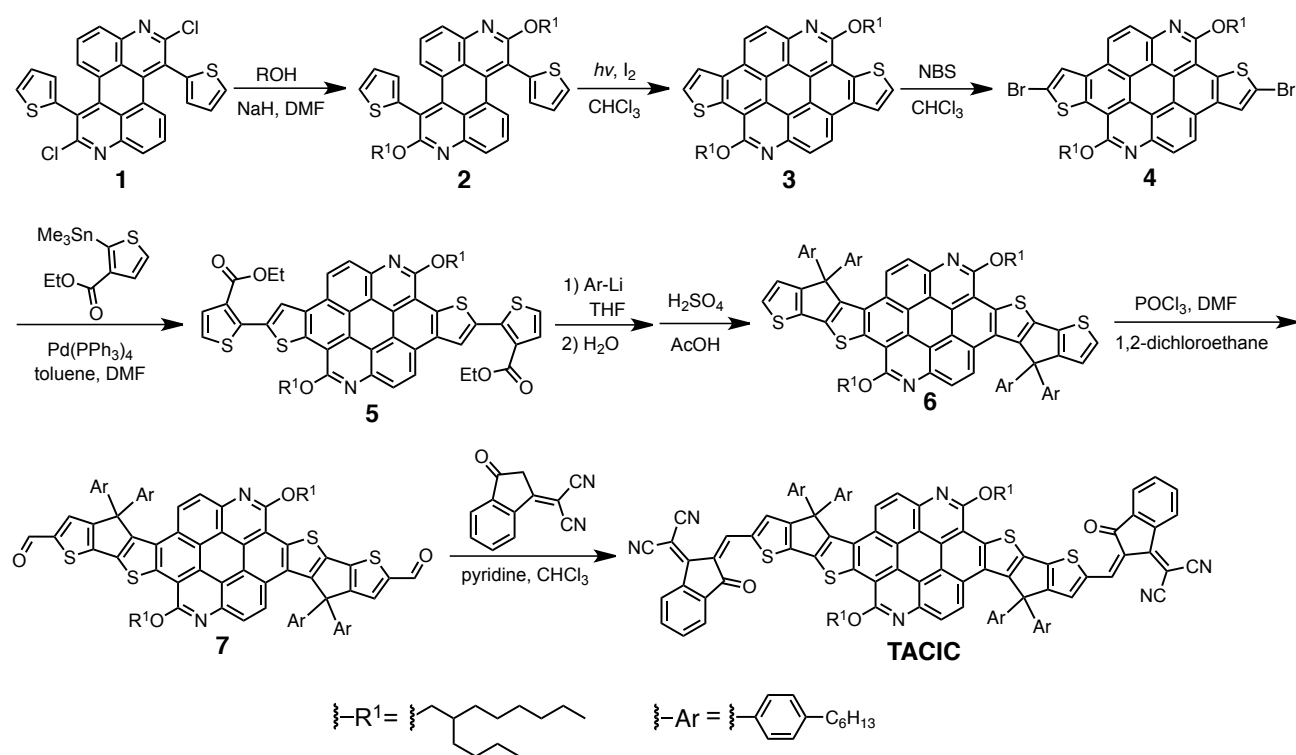
Solubility tests. The solubility of NFA in chloroform was estimated as follows. First, the absorption spectra of NFA chloroform solutions with three different concentrations were measured. A linear correlation between the concentration and the absorbance was found, agreeing well with Beer–Lambert law. Next saturated solution of NFA was prepared by adding an excess amount of the compound to chloroform, followed by sonication at room temperature for 10 min. After the saturated solution was filtered through a membrane filter (Cosmonice Filter S, COSMOSIL, pore size: 0.45 μm) to remove the aggregates, the filtrate was diluted 2500 times with chloroform and the absorption spectrum of the diluted solution was measured. The concentration of the diluted solution was calculated from a linear correlation between the concentration and the absorbance.

GIWAXS measurements. Samples were prepared by spin-coating the NFA or PBDB-T:NFA solution on the ITO/ZnO substrate as conducted in the OPV device fabrications. GIWAXS measurements were conducted at the SPring-8 on beamline BL46XU. The sample was irradiated at a fixed incident angle on the order of 0.12° through a Huber diffractometer with X-ray energy of 12.398 keV (X-ray wavelength $\lambda = 0.10002$ nm), and the GIWAXS patterns were recorded with a 2D image detector (Pilatus 300 K) with the sample-to-detector distances of 173.8 mm.

Synthetic Procedures

Materials. 1,7-Dithienyl-2,8-dichloro-3,9-diazaperylene (compound **1**),^{S2} ethyl 2-(trimethylstannyl)thiophene-3-carboxylate,^{S3} tetrakis(triphenylphosphine)palladium(0) ($\text{Pd}(\text{PPh}_3)_4$),^{S4} and 1,1-dicyanomethylene-3-indanone (IC)^{S5} were synthesized according to the literature procedures. PBDB-T and ITIC were purchased from 1-Material. All other chemicals were purchased from commercial supplier and used without further purification.

Synthesis.



Scheme S1. Synthetic route for TACIC.

Compound 2. Compound **2** was synthesized according to a slightly modified literature procedure.^{S2} To a solution of compound **1** (2.02 g, 4.14 mmol, 1.0 equiv.) and NaH in oil (50–72%, 610 mg, 13–18 mmol, 3.0–4.4 equiv.) in DMF (30 mL), 2-butyl-1-octanol (2.44 mL, 10.9 mmol, 2.6 equiv.) was added at 0°C under an Ar atmosphere. The mixture was stirred at room temperature overnight and then quenched with water. The reaction was extracted with CHCl_3 , the organic phase was dried over Na_2SO_4 . After filtration, the solvent was removed under reduced pressure, and the resulting residue was purified by column chromatography with hexane/ $\text{CHCl}_3 = 1:1$ as eluent. Compound **2** was

obtained as a yellow oil. Ring closure reaction partially occurred during the purification process, resulting in a mixture of compound **2**, mono annulated compound, and compound **3**. The mixture was all used directly for the following ring closure reaction without further purification.

Compound 3. Compound **3** was synthesized according to a slightly modified literature procedure.^{S2} A mixed solution of **2**, the mono annulated compound, and **3** in CHCl₃ (300 mL) was irradiated with a 300 W incandescent lamp with catalytic amount of iodine for 2 days under an Ar atmosphere. The reaction mixture was quenched with Na₂SO₃ aq., extracted with CHCl₃, and then the organic phase was washed with brine and dried over Na₂SO₄. After filtration, the solvent was removed under reduced pressure, and the resulting residue was purified by column chromatography with hexane/CHCl₃ = 1:1 as eluent to give a yellow solid, which was further purified by reprecipitation with CHCl₃/ethanol. Compound **3** was obtained as a yellow solid (1.44 g, yield: 44.4% in 2 steps). ¹H NMR (400 MHz, CDCl₃, ppm): δ 8.05 (d, *J* = 8.8 Hz, 2H), 7.87 (m, 4H), 7.77 (d, *J* = 5.2 Hz, 2H), 4.76 (d, *J* = 5.2 Hz, 4H), 2.26 (m, 2H), 2.00 (m, 4H), 1.84–1.76 (m, 4H), 1.73–1.67 (m, 8H), 1.63–1.42 (m, 16H), 1.10 (t, *J* = 7.2 Hz, 6H), 0.98 (t, *J* = 7.2 Hz, 6H). ¹³C NMR (100 MHz, CDCl₃, ppm): δ 156.91, 139.07, 134.91, 131.00, 127.70, 126.65, 124.52, 123.84, 122.73, 121.24, 117.64, 113.74, 109.95, 70.03, 38.30, 32.30, 32.03, 31.71, 30.19, 29.85, 29.64, 27.41, 23.55, 23.21, 23.03, 22.86, 14.58, 14.41, 14.29. HRMS (p MALDI) calcd for [C₅₀H₅₈N₂O₂S₂+H]⁺: 783.4012; found: 783.3992. IR (ATR, cm⁻¹): ν_{max} 2950, 2920, 2852, 2187, 2165, 1974, 1567, 1483, 1462, 1421, 1391, 1337, 1293, 1230, 1187, 1152, 1109, 1042, 973, 933, 869, 825, 716, 692, 644, 584, 566, 510. Melting point: 162–164 °C.

Compound 4. Compound **4** was synthesized according to a slightly modified literature procedure.^{S6} A solution of compound **3** (1.11 g, 1.42 mmol, 1.0 equiv.) and *N*-bromosuccinimide (NBS, 1.01 g, 5.68 mmol, 4.0 equiv.) in CHCl₃ (70 mL) was stirred overnight at room temperature under an Ar atmosphere. The reaction was quenched with water and then the mixture was extracted with CHCl₃, the organic phase was dried over Na₂SO₄. After filtration, the solvent was removed under reduced pressure. The resulting residue was purified by column chromatography with hexane/CHCl₃ = 1:1 as eluent to give a solid, which was further purified by reprecipitation with CHCl₃/ethanol. Compound

4 was obtained as a dark green solid (1.33 g, yield: 99.7%). ¹H NMR (400 MHz, CDCl₃, ppm): δ 7.52 (s, 2H), 7.45 (s, 4H), 4.56 (m, 4H), 2.18 (m, 2H), 1.88 (m, 4H), 1.70–1.50 (m, 28H), 1.17–1.13 (m, 6H), 1.04–1.02 (m, 6H). ¹³C NMR (100 MHz, CDCl₃, ppm): δ 154.76, 137.23, 132.92, 130.37, 125.43, 123.03, 121.35, 120.83, 120.52, 116.58, 114.83, 110.73, 106.95, 69.94, 37.98, 32.38, 31.81, 31.42, 31.10, 30.21, 29.90, 29.54, 27.36, 23.56, 23.10, 14.66, 14.53, 14.34. HRMS (p MALDI) calcd for [C₅₀H₅₆Br₂N₂O₂S₂+H]⁺: 939.2223; found: 939.2212. IR (ATR, cm⁻¹): ν_{max} 2953, 2920, 2853, 2373, 2353, 2206, 2020, 1999, 1957, 1569, 1502, 1482, 1463, 1420, 1394, 1377, 1337, 1292, 1215, 1188, 1150, 1107, 1047, 974, 920, 814, 791, 726, 689, 560, 493. Melting point: 205–209 °C.

Compound 5. A solution of compound **4** (474 mg, 0.504 mmol, 1.0 equiv.) and ethyl 2-(trimethylstannyl)thiophene-3-carboxylate (1.15 mL, 5.05 mmol, 10 equiv.) in toluene (20 mL) and DMF (5 mL) was deoxygenated with Ar for 30 min. After Pd(PPh₃)₄ (56.3 mg, 0.0487 mmol, 0.1 equiv.) was added to the mixture, the reaction mixture was stirred overnight at 110 °C. The reaction was quenched with KF aq., extracted with CHCl₃, and the organic phase was dried over Na₂SO₄. After filtration, the solvent was removed under reduced pressure and the resulting residue was purified by column chromatography with hexane/CHCl₃ = 1:1 to 0:1 as eluent. The crude product of compound **5** was obtained as an orange solid and used in the next step without further purification.

Compound 6. To a solution of 4-hexyl-1-bromobenzene (2.00 mL, 9.79 mmol, 19 equiv.) in THF (40 mL) at -78 °C, *n*-BuLi (1.57 M, 6.25 mL, 9.81 mmol, 19 equiv.) was added under an Ar atmosphere, before stirred at -78 °C for 1 h. A solution of crude product of compound **5** (less than 0.504 mmol, 1 equiv.) in THF (100 mL) was added slowly. After the addition, the mixture was stirred at -78 °C for 1 h and then at room temperature for 3 h. The reaction was quenched with water, extracted with CHCl₃, and combined organic phase was dried over Na₂SO₄. After filtration, the solvent was removed under reduced pressure. The crude product was obtained and used in the next step without further purification. To a solution of crude product in acetic acid (100 mL), H₂SO₄ (1 mL) was added, before stirred at 80 °C for 30 min. The reaction was quenched with Na₂CO₃ aq., extracted with CHCl₃, and combined organic phase was dried over Na₂SO₄. After filtration, the solvent was removed under reduced pressure, and the resulting residue was purified by column

chromatography with hexane/CHCl₃ = 1:0 to 4:1 as eluent. Compound **6** was obtained as an orange solid (262 mg, yield: 32.2% in 3 steps). ¹H NMR (400 MHz, CDCl₃, ppm): δ 8.97 (d, *J* = 9.2 Hz, 2H), 8.37 (d, *J* = 9.2 Hz, 2H), 7.55 (d, *J* = 8.0 Hz, 8H), 7.28 (d, *J* = 5.2 Hz, 2H), 7.17 (d, *J* = 5.2 Hz, 2H), 7.03 (d, *J* = 8.4 Hz, 8H), 5.02 (d, *J* = 5.6 Hz, 4H), 2.48 (m, 8H), 2.34 (m, 2H), 1.90 (m, 4H), 1.72 (m, 4H), 1.63–1.42 (m, 24H), 1.35 (m, 8H), 1.26–1.17 (m, 24H), 1.00 (t, *J* = 7.2 Hz, 6H), 0.87 (t, *J* = 7.2 Hz, 6H), 0.80 (t, *J* = 6.4 Hz, 12H). ¹³C NMR (100 MHz, CDCl₃, ppm): δ 164.22, 158.27, 152.98, 142.70, 141.90, 141.77, 140.16, 136.38, 136.12, 135.32, 134.84, 133.12, 129.22, 128.84, 128.46, 127.66, 126.65, 126.51, 126.36, 125.06, 123.28, 120.98, 115.90, 112.59, 70.68, 64.38, 64.19, 38.16, 35.63, 33.92, 32.13, 31.97, 31.80, 31.68, 31.28, 31.11, 29.99, 29.45, 29.19, 27.19, 23.37, 22.88, 22.68, 22.53, 14.46, 14.33, 14.19, 14.03. HRMS (APCI) calcd for [C₁₀₈H₁₂₆N₂O₂S₄]⁺: 1610.8697; found: 1610.8666. IR (ATR, cm⁻¹): ν_{max} 3697, 2922, 2853, 2801, 2363, 2321, 2298, 2192, 1984, 1928, 1559, 1507, 1452, 1426, 1379, 1329, 1281, 1214, 1184, 1093, 1020, 968, 915, 827, 718, 686, 651, 568, 518. Melting point: 183–184 °C.

Compound 7. Vilsmeier reagent was prepared according to the following procedure. POCl₃ (0.37 mL, 3.97 mmol, 60 equiv.) was added to a solution of DMF (14 mL) at 0 °C and stirred at 0 °C for 1 h under an Ar atmosphere. To a solution of compound **6** (108 mg, 0.0667 mmol, 1.0 equiv.) in 1,2-dichloroethane (10 mL), the Vilsmeier reagent was added at 0 °C. The mixture was stirred at room temperature for 2 h and then at 80 °C for 2 h. After cooling down to room temperature, the reaction was quenched with AcONa aq., extracted with CHCl₃, and the organic phase was dried over Na₂SO₄. After filtration, the solvent was removed under reduced pressure, and the resulting residue was purified by column chromatography with CHCl₃ as eluent to give a solid, which was further purified by reprecipitation with CHCl₃/ethanol. Compound **7** was obtained as an orange solid (83.0 mg, yield: 74.6%). ¹H NMR (400 MHz, CDCl₃, ppm): δ 9.84 (s, 2H), 8.98 (d, *J* = 8.8 Hz, 2H), 8.40 (d, *J* = 9.2 Hz, 2H), 7.80 (s, 2H), 7.54 (d, *J* = 8.4 Hz, 8H), 7.07 (d, *J* = 8.0 Hz, 8.4H), 5.03 (d, *J* = 5.2 Hz, 4H), 2.50 (m, 8H), 2.35 (m, 2H), 1.95–1.84 (m, 4H), 1.75–1.71 (m, 4H), 1.63–1.18 (m, 72H), 1.00 (t, *J* = 7.2 Hz, 6H), 0.86 (t, *J* = 7.2 Hz, 6H), 0.80 (t, *J* = 7.2 Hz, 12H). ¹³C NMR (100 MHz, CDCl₃, ppm): δ 182.76, 163.997, 158.45, 156.69, 145.58, 145.52, 142.53, 141.19, 140.84, 137.42, 134.83, 132.63,

131.71, 129.10, 128.73, 127.46, 127.04, 125.14, 121.11, 115.69, 112.50, 70.98, 64.43, 38.11, 35.60, 32.08, 31.91, 31.76, 31.66, 31.25, 29.96, 29.38, 29.13, 27.14, 23.34, 22.86, 22.66, 14.44, 14.30, 14.17. HRMS (APCI) calcd for $[C_{110}H_{126}N_2O_4S_4]^+$: 1666.8595; found 1666.8595. IR (ATR, cm^{-1}): ν_{max} 3688, 2954, 2907, 2887, 2585, 2508, 2363, 2195, 2173, 2140, 2094, 1979, 1661, 1454, 1418, 1279, 1221, 1139, 1094, 826, 653, 609. Melting point: 254–256 °C.

TACIC. A solution of compound **7** (55.7 mg, 0.0334 mmol, 1.0 equiv.) and IC (63.9 mg, 0.329 mmol, 10 equiv.) in $CHCl_3$ (7 mL) was deoxygenated with Ar for 30 min before 1 drop of pyridine was added. After overnight refluxing, the crude product was reprecipitated with $CHCl_3$ /EtOH, and the resulting residue was purified by column chromatography with hexane/ $CHCl_3$ = 1:2 as eluent, reprecipitated with $CHCl_3$ /EtOH again. TACIC was obtained as a dark blue solid (75.3 mg, yield: 89.6%). 1H NMR (400 MHz, $CDCl_3$, ppm): δ 8.99 (d, J = 9.2 Hz, 2H), 8.91 (s, 2H), 8.66 (m, 2H), 8.41 (d, J = 9.2 Hz, 2H), 7.90 (m, 2H), 7.80 (s, 2H), 7.72 (m, 4H), 7.57 (d, J = 8.4 Hz, 8H), 7.09 (d, J = 8.0 Hz, 8H), 5.05 (d, J = 5.2 Hz, 4H), 2.51 (m, 8H), 2.38 (m, 2H), 1.94–1.70 (m, 8H), 1.62–1.18 (m, 56H), 1.00 (t, J = 7.2 Hz, 6H), 0.90–0.78 (m, 18H). ^{13}C NMR (100 MHz, $CDCl_3$, ppm): δ 188.39, 164.92, 158.90, 154.97, 142.74, 141.89, 141.23, 140.93, 139.74, 138.88, 138.26, 134.56, 133.92, 132.45, 129.54, 129.17, 128.92, 127.73, 127.27, 125.21, 121.12, 121.00, 115.53, 115.17, 71.14, 68.33, 64.23, 37.89, 35.64, 32.12, 31.98, 31.77, 31.26, 29.98, 29.85, 29.31, 29.18, 27.07, 23.34, 22.86, 22.66, 14.42, 14.31, 14.17. HRMS (p MALDI) calcd for $[C_{134}H_{134}N_6O_4S_4]^+$: 2018.9344; found: 2018.9299. IR (ATR, cm^{-1}): ν_{max} 2949, 2910, 2853, 2188, 2164, 1974, 1694, 1537, 1481, 1400, 1307, 1293, 1250, 1222, 1177, 1129, 1092, 980, 911, 830, 768, 720, 690, 596, 513.

Supporting Notes

Decay dynamics of singlet excited state of TACIC in solution and film states. Fig.3a shows the transient absorption spectra of the TACIC chloroform solution measured at 0–500 ps in NIR region. Immediately after the photoexcitation at 650 nm, an absorption band was observed at 1080 nm. We therefore assign this absorption band to the singlet excited state (S_1) of TACIC.

In transient absorption measurements under relatively strong excitation intensities, bimolecular deactivation processes of singlet excited states, such as singlet–singlet exciton annihilation, can produce additional decay channels, which are not essential under the 1 Sun condition. Such bimolecular deactivation processes possess rate constants that are dependent on the excitation laser intensity. Transient absorption profiles corresponding to S_1 of TACIC in solution are shown in Fig. S7a. The detection wavelength was 1050 nm, and the excitation intensities were 26 and 11 $\mu\text{J cm}^{-2}$. The decay dynamics of S_1 of TACIC in solution was independent of the excitation intensity, suggesting that the bimolecular deactivation processes for S_1 of TACIC in solution were absent. The main decay component has a lifetime of 220 ps (Fig. S7a). In addition, both the decay profiles with excitation intensities of 26 and 11 $\mu\text{J cm}^{-2}$ displayed a minor component with a relatively short lifetime of <5 ps (Fig. S7b). This can be attributed to the structural change in the excited state; a change in the molecular configuration of TACIC in the excited state causes a small change in the absorption coefficient.

Fig. 3b displays the transient absorption spectra of the TACIC film measured at 0–1000 ps in visible and NIR regions. Immediately after the photoexcitation at 700 nm, absorption bands were observed at 570 nm, 750 nm, and 1080 nm. We therefore assign these absorption bands to S_1 of the TACIC film. In addition, negative peaks also appeared at 650 nm and 710 nm immediately after the photoexcitation, which can be attributed to the ground state bleaching (GSB) of the TACIC film.

Transient absorption profiles corresponding to S_1 of the TACIC film are shown in Fig. S7c. The detection wavelength was 1100 nm and the excitation intensity ranged from 0.68 to 2.8 $\mu\text{J cm}^{-2}$. At >150 ps, the decay dynamics of S_1 of the TACIC film was independent of the excitation intensity, suggesting that the bimolecular deactivation processes for S_1 of the TACIC film were absent in this

time region. On the other hand, the decay dynamics of S_1 of the TACIC film was apparently affected by the excitation intensity at <150 ps, indicating the presence of the bimolecular deactivation processes such as singlet–singlet exciton annihilation in this time region. Therefore, we calculated the lifetime of S_1 of the TACIC film from the transient absorption profiles at >150 ps and obtained the value of 1.59 ns.

Decay dynamics of S_1 of ITIC in solution and film states. Fig. S8a shows the transient absorption spectrum of the ITIC chloroform solution measured at 0–500 ps in NIR region. Immediately after the photoexcitation at 650 nm, an absorption band was observed at 940 nm, which was attributable to S_1 of ITIC. This assignment agrees with literatures.^{S7} Transient absorption profiles corresponding to S_1 of ITIC in solution are shown in Fig. S8b. The detection wavelength was 950 nm and the excitation intensities were 26 and 11 $\mu\text{J cm}^{-2}$. The decay dynamics of S_1 of ITIC in solution was independent of the excitation intensity, suggesting that the bimolecular deactivation processes for S_1 of ITIC in solution were absent. The main decay component has a lifetime of 176 ps (Fig. S8b). In addition, both the decay profiles with the excitation intensities of 26 and 11 $\mu\text{J cm}^{-2}$ displayed a minor component with a relatively short lifetime of <5 ps (Fig. S8c), as in the case of TACIC. This short lifetime component can also be attributed to the structural change in the excited state.

Fig. S8d displays the transient absorption spectrum of the ITIC film measured at 0–100 ps in visible and NIR regions. Immediately after the photoexcitation at 700 nm, an absorption band of S_1 of the ITIC film was observed at 960 nm. In addition, negative peaks also appeared at 650 nm and 720 nm immediately after the photoexcitation, which can be attributed to the ground state bleaching (GSB) of the ITIC film. Transient absorption profiles corresponding to S_1 of the ITIC film are shown in Fig. S8e. The detection wavelength was 950 nm and the excitation intensity ranged from 0.68 to 2.8 $\mu\text{J cm}^{-2}$. At >10 ps, the decay dynamics of S_1 of the ITIC film was independent of the excitation intensity, suggesting that the bimolecular deactivation processes for S_1 of ITIC film were absent in this time region. On the other hand, the decay dynamics of S_1 of the ITIC film was apparently affected by the excitation intensity at <10 ps, indicating the presence of the bimolecular deactivation processes in this

time region, in addition to the fast structural change. Therefore, we calculated the lifetime of S_1 of the ITIC film from the transient absorption profiles at >10 ps and obtained the value of 29.2 ps.

Signal assignments in transient absorption spectra of PBDB-T:TACIC and PBDB-T:ITIC. Fig. 5a shows the transient absorption spectra of the PBDB-T:TACIC blend film measured at 0–2500 ps. Immediately after the photoexcitation at 700 nm, at which TACIC was predominantly excited, absorption bands were observed at 550, 750, and 1080 nm, which can be assigned to S_1 of TACIC. In addition, negative peaks also appeared at 650 and 710 nm due to the GSB of TACIC (Fig. S11). The transient absorption spectrum at 2500 ps exhibited broad absorption bands at 500–1000 nm with a shoulder around 950 nm (Fig. 5a), although the S_1 signals of TACIC at 550 and 1080 nm already disappeared. To explore the origin of the absorption bands at 500–1000 nm, first we observed the changes in absorption spectra of TACIC by chemical reduction with cobaltocene (Fig. S14a–c). When adding an equivalent amount of cobaltocene to TACIC solution in benzonitrile, the differential absorption spectrum showed an intense negative peak at 680 nm and positive peaks at 770 and 910 nm (Fig. S14b,c). Then, we also implemented the chemical oxidation of PBDB-T using magic blue (tris(4-bromophenyl)ammoniumyl hexachloroantimonate) as an oxidant and observed the changes in absorption spectrum of PBDB-T (Fig. S14d,e). When adding 9.5×10^{-9} mol of magic blue in CH_2Cl_2 (10 μL) to PBDB-T (4.2×10^{-8} mol by repeating unit) in CHCl_3 (3 mL), the differential absorption spectrum showed negative peaks at 580 and 630 nm and positive peaks at 700 and 930 nm (Fig. S14d,e). Considering these results, we assign the positive absorption bands in the transient absorption spectrum of PBDB-T:TACIC at 2500 ps to both the TACIC radical anion and the PBDB-T hole polaron.^{S8} The negative signal at 710 nm is attributed to the TACIC radical anion. All the assignments confirmed the formation of the charge transfer (CT) and charge dissociated (CD) states.

Fig. 5b displays the transient absorption spectra of the PBDB-T:ITIC blend film measured at 0–2500 ps. Immediately after the photoexcitation at 700 nm, at which ITIC was predominantly excited, an absorption band was observed at 960 nm, which was attributable to S_1 of ITIC. The transient absorption spectrum of PBDB-T:ITIC at 2500 ps showed a broad absorption band with a peak at 930

nm. We observed the changes in absorption spectra of ITIC by chemical reduction with cobaltocene, and only a negative absorption at 690 nm was detected. As discussed for the transient absorption spectra of the PBDB-T:TACIC blend film, negative peaks at 580, 630 nm and a positive peak at 930 nm are assigned to the PBDB-T hole polaron (Fig. S14e), whereas a negative peak at 700 nm is attributed to the ITIC radical anion. Considering the similarity in the molecular structures of ITIC and TACIC, the ITIC radical anion may also contribute to the absorption band at 930 nm.

Decay dynamics of S_1 of TACIC and charge-separated states in PBDB-T:TACIC with various excitation intensities. Transient absorption profiles corresponding to S_1 of TACIC in the PBDB-T:TACIC blend film are shown in Fig. S15a. The detection wavelength was 550 nm, and the excitation intensity ranged from 2.1 to 15.8 $\mu\text{J cm}^{-2}$. The S_1 decay dynamics of TACIC was independent of the excitation intensity at $<7.5 \mu\text{J cm}^{-2}$, suggesting that the bimolecular deactivation processes for S_1 of TACIC were absent. The lifetime of S_1 of TACIC was ca. 60 ps with the excitation intensity of $<7.5 \mu\text{J cm}^{-2}$.

On the other hand, relatively strong excitation intensities can also lead to bimolecular deactivation processes of polarons, e.g., nongeminate charge recombination, which are ignorable at the time region of <3000 ps under the 1 Sun condition. Transient absorption profiles corresponding to both the PBDB-T hole polaron and the TACIC radical anion in the PBDB-T:TACIC blend film are shown in Fig. S15b. The detection wavelength was 950 nm and the excitation intensity ranged from 3.8 to 15.8 $\mu\text{J cm}^{-2}$. Apparently, the decay profile with the excitation intensity of 15.8 $\mu\text{J cm}^{-2}$ was different from that with 7.5 $\mu\text{J cm}^{-2}$; the faster decay with the excitation intensity of 15.8 $\mu\text{J cm}^{-2}$ at <500 ps indicates the occurrence of the bimolecular deactivation processes of the PBDB-T hole polaron and the TACIC radical anion. In addition, the decay profile with the excitation intensity of 3.8 $\mu\text{J cm}^{-2}$ was noisy due to the low absorption intensity and the insufficient detection sensitivity in the NIR region. Therefore, to diagnose the presence of the bimolecular deactivation processes of the PBDB-T hole polaron with the excitation intensity of 7.5 $\mu\text{J cm}^{-2}$, we decided to monitor the GSBs of PBDB-T and TACIC in the visible region, i.e., at 630 nm, at 0–2800 ps (Fig. S15c). The time profiles of the GSB were

independent of the excitation intensities of 3.8–7.5 $\mu\text{J cm}^{-2}$, indicating the mono-molecular processes of the relaxation to the ground states. Furthermore, the decay time profile of the PBDB-T hole polaron and the TACIC radical anion with the excitation energy of 7.5 $\mu\text{J cm}^{-2}$ coincides with the time profiles of the GSB recovery with the excitation intensities of 3.8–7.5 $\mu\text{J cm}^{-2}$ at >500 ps (Fig. S15c). This indicates the absence of the bimolecular deactivation processes of the PBDB-T hole polaron and the TACIC radical anion with the excitation energy of 7.5 $\mu\text{J cm}^{-2}$. Therefore, we can estimate the charge dissociation efficiency from the decay profiles of the PBDB-T hole polaron and the TACIC radical anion with the excitation energy of 7.5 $\mu\text{J cm}^{-2}$ (see the main text).

Decay dynamics of S_1 of ITIC and charge-separated states in PBDB-T:ITIC with various excitation intensities. Although the S_1 of ITIC showed a relatively strong absorption band at 960 nm in the transient absorption spectrum of PBDB-T:ITIC (Fig. 5b), the substantial overlapping with the band of the PBDB-T hole polaron and the ITIC radical anion complicated the estimation of the S_1 lifetime of ITIC by monitoring the transient absorption intensity at 960 nm. Instead, we monitored GSB of PBDB-T at 580 nm with the excitation intensities of 2.1–15.8 $\mu\text{J cm}^{-2}$ (Fig. S16). Fig. S16a displays the time profiles at 0–100 ps. Because ITIC predominantly absorbed the excitation light at 700 nm, the GSB of PBDB-T at 580 nm originated from the interaction of PBDB-T with the excited ITIC, i.e., charge transfer. The GSB of PBDB-T was observed even at 0 ps, indicative of the immediate charge transfer on laser irradiation. This suggests that there exist sufficiently small ITIC domains for excitons to immediately contact the donor–acceptor interface. After the photoexcitation, the GSB signal of PBDB-T grew with the time constant of ca. 7 ps (Fig. S16a), indicating that S_1 of ITIC decayed with this time constant. Therefore, we estimated the S_1 decay constants of ITIC in PBDB-T:ITIC to be <100 fs (beyond the time resolution of the instrument) and 7 ps (see the main text). At the excitation intensity of 15.8 $\mu\text{J cm}^{-2}$, the GSB signal of PBDB-T clearly showed a decay at >20 ps, suggesting the occurrence of bimolecular deactivation processes of PBDB-T hole polaron such as nongeminate recombination due to the relatively strong excitation intensity. Fig. S16b depicts the time profiles of the PBDB-T GSB at 0–2800 ps. The dynamics was independent of the excitation

intensity of $<7.5 \mu\text{J cm}^{-2}$, suggesting that the bimolecular deactivation processes for PBDB-T hole polaron were absent in this time scale. Therefore, we can estimate the charge dissociation efficiency from the GSB recovery profiles of PBDB-T at 580 nm with the excitation energy of $<7.5 \mu\text{J cm}^{-2}$ (see the main text).

Table S1 Charge mobilities (μ_e and μ_h) and charge mobility balances (μ_e/μ_h).

sample	μ_e^a of single-component film / $\times 10^{-4} \text{ cm}^2 \text{ V}^{-1} \text{ s}^{-1}$	μ_e^b of blend film with PBDB-T / $\times 10^{-4} \text{ cm}^2 \text{ V}^{-1} \text{ s}^{-1}$	μ_h^c of blend film with PBDB-T / $\times 10^{-4} \text{ cm}^2 \text{ V}^{-1} \text{ s}^{-1}$	μ_e/μ_h of blend film with PBDB-T
TACIC	6.2	1.2	2.6	0.46
ITIC	2.6	3.1	2.1	1.5

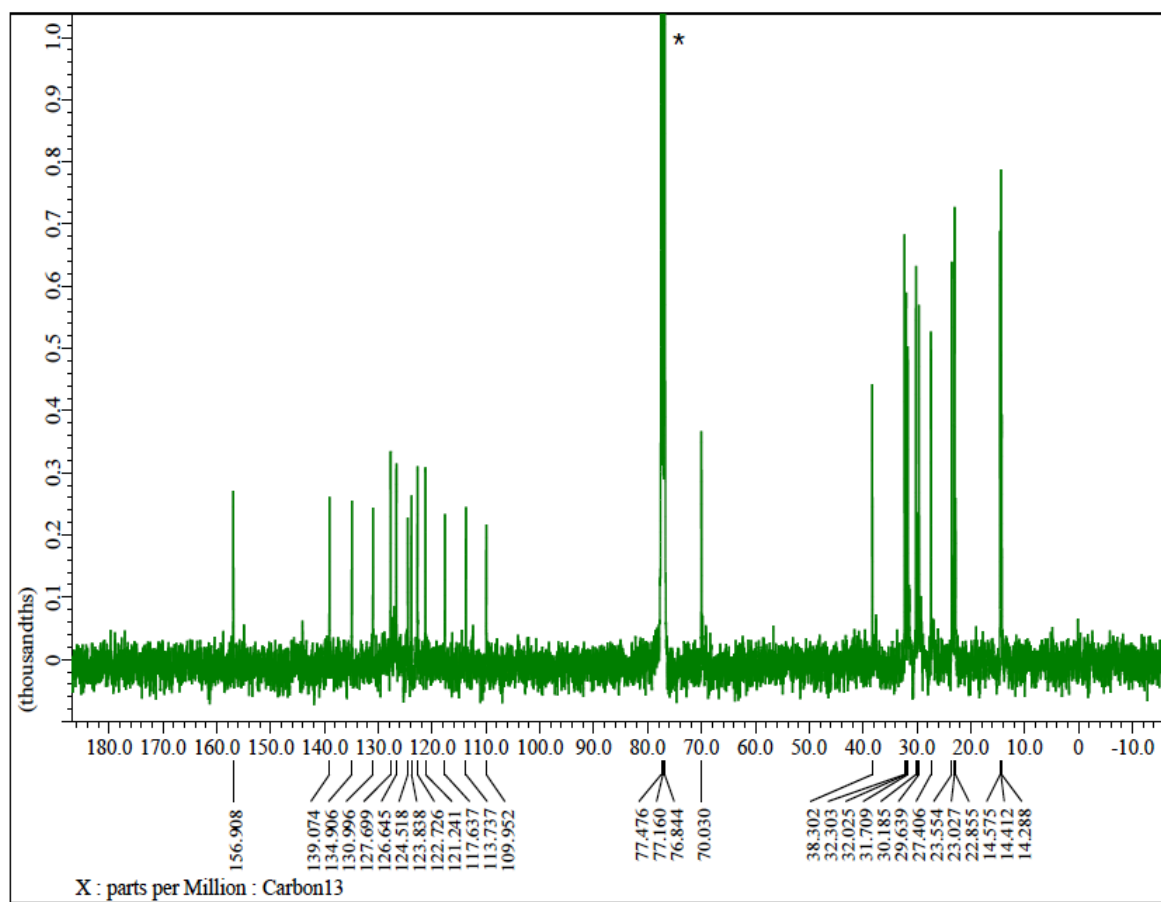
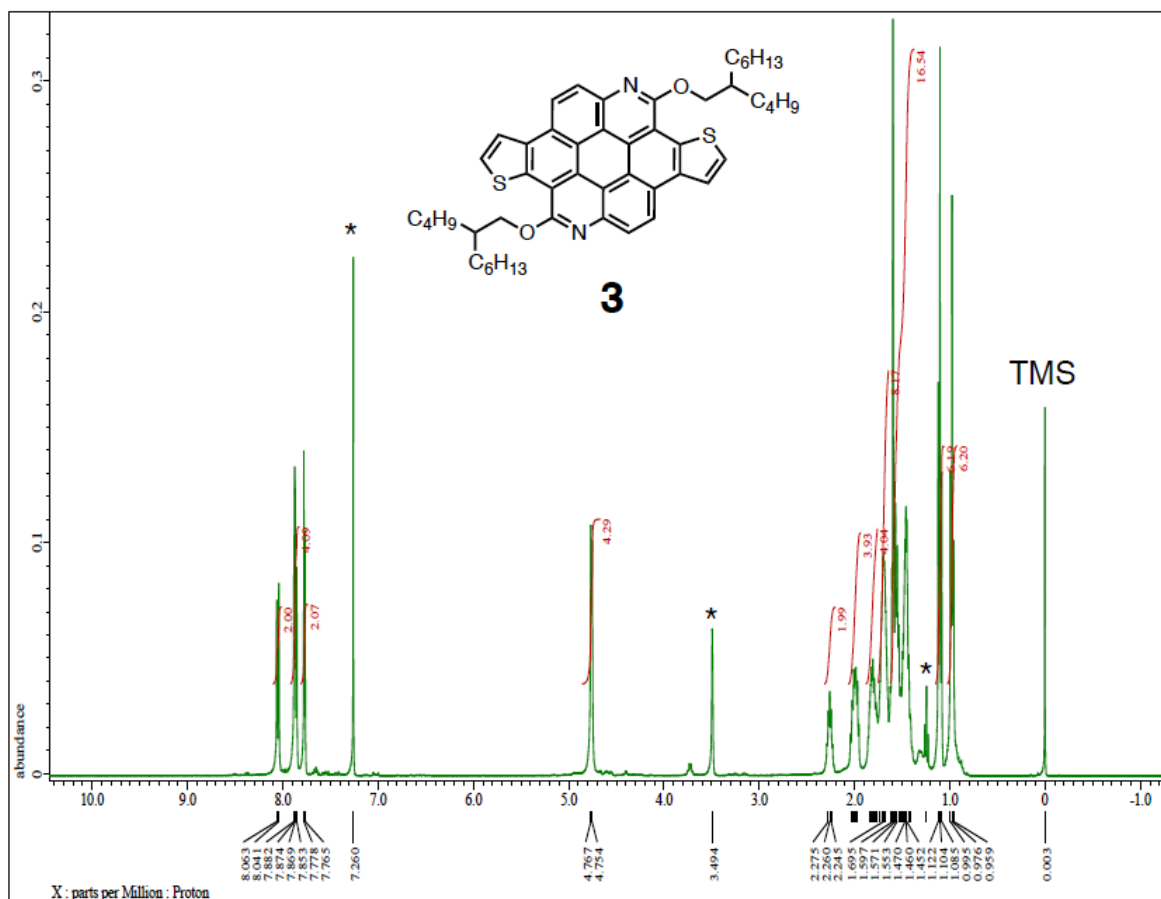
^a Measured by SCLC with the device configuration of ITO/ZnO/NFA/Al. ^b Device configuration; ITO/ZnO/PBDB-T:NFA/Al. ^c Device configuration; ITO/PEDOT:PSS/PBDB-T:NFA/MoO₃/Au.

Table S2 Photoluminescence quantum yield (Φ_{PL}),^a singlet exciton lifetime (τ_{S_1}),^b radiative rate constant (k_{r}),^c and nonradiative rate constant (k_{nr})^c of TACIC and ITIC in solution and film states.

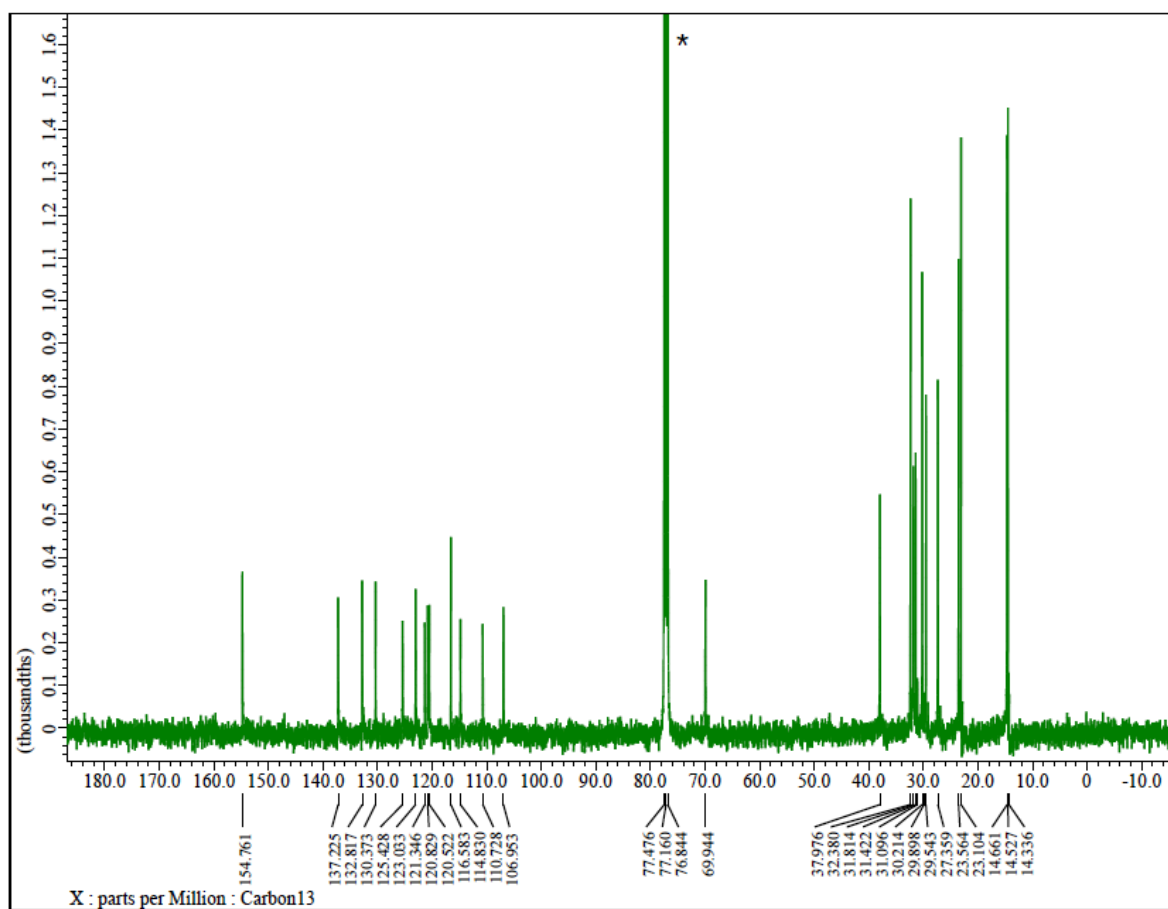
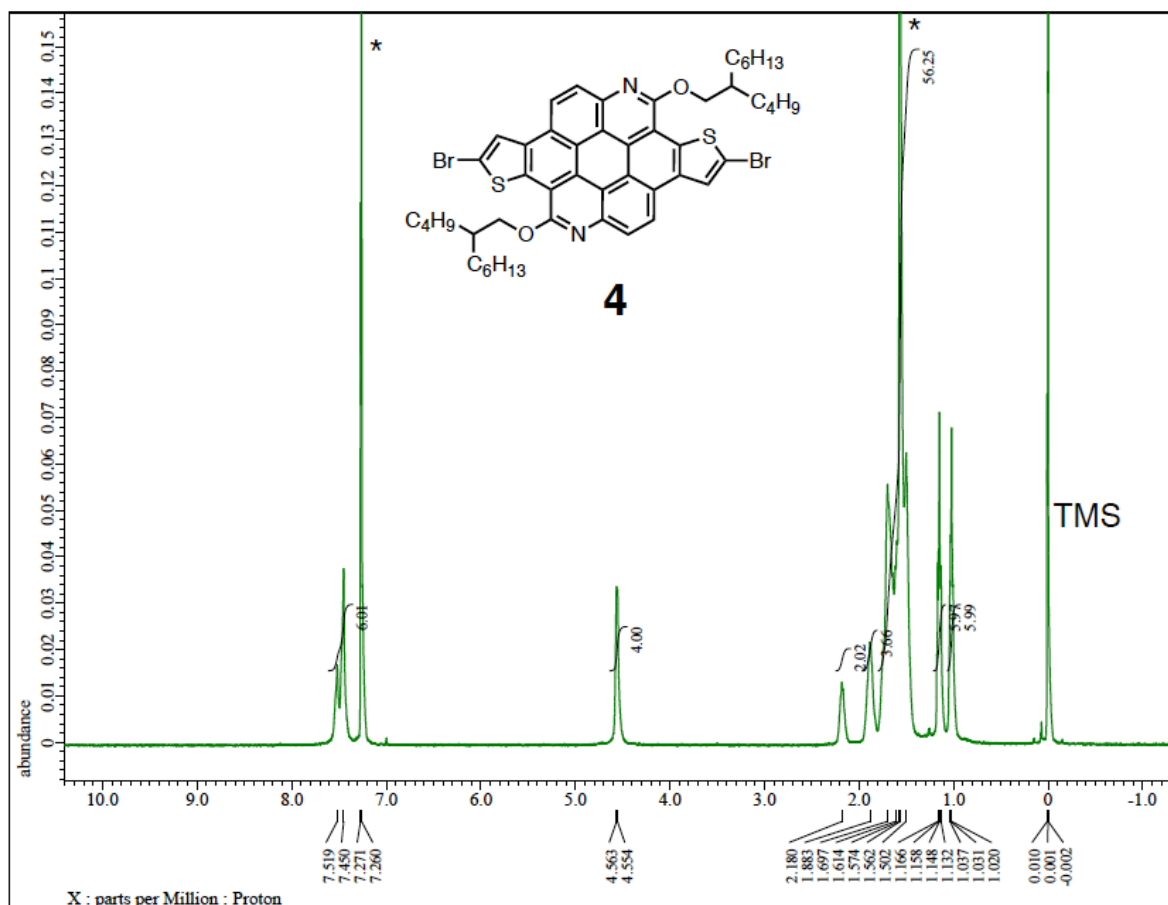
sample	Φ_{PL}	$\tau_{\text{S}_1} / \text{ps}$	$k_{\text{r}} / \text{s}^{-1}$	$k_{\text{nr}} / \text{s}^{-1}$
TACIC solution	0.065	220	3.0×10^8	4.2×10^9
TACIC film	0.077	1590	4.8×10^7	5.8×10^8
ITIC solution	0.063	176	3.6×10^8	5.3×10^9
ITIC film	0.022	29.2	7.5×10^8	3.3×10^{10}

^a Estimated by the integrated sphere method. ^b Estimated by the transient absorption spectroscopy. ^c k_{r} and k_{nr} are calculated from the experimental data of Φ_{PL} and τ_{S_1} , according to the following equations; $\Phi_{\text{PL}} = k_{\text{r}} \times (k_{\text{r}} + k_{\text{nr}})^{-1}$ and $\tau_{\text{S}_1} = (k_{\text{r}} + k_{\text{nr}})^{-1}$.

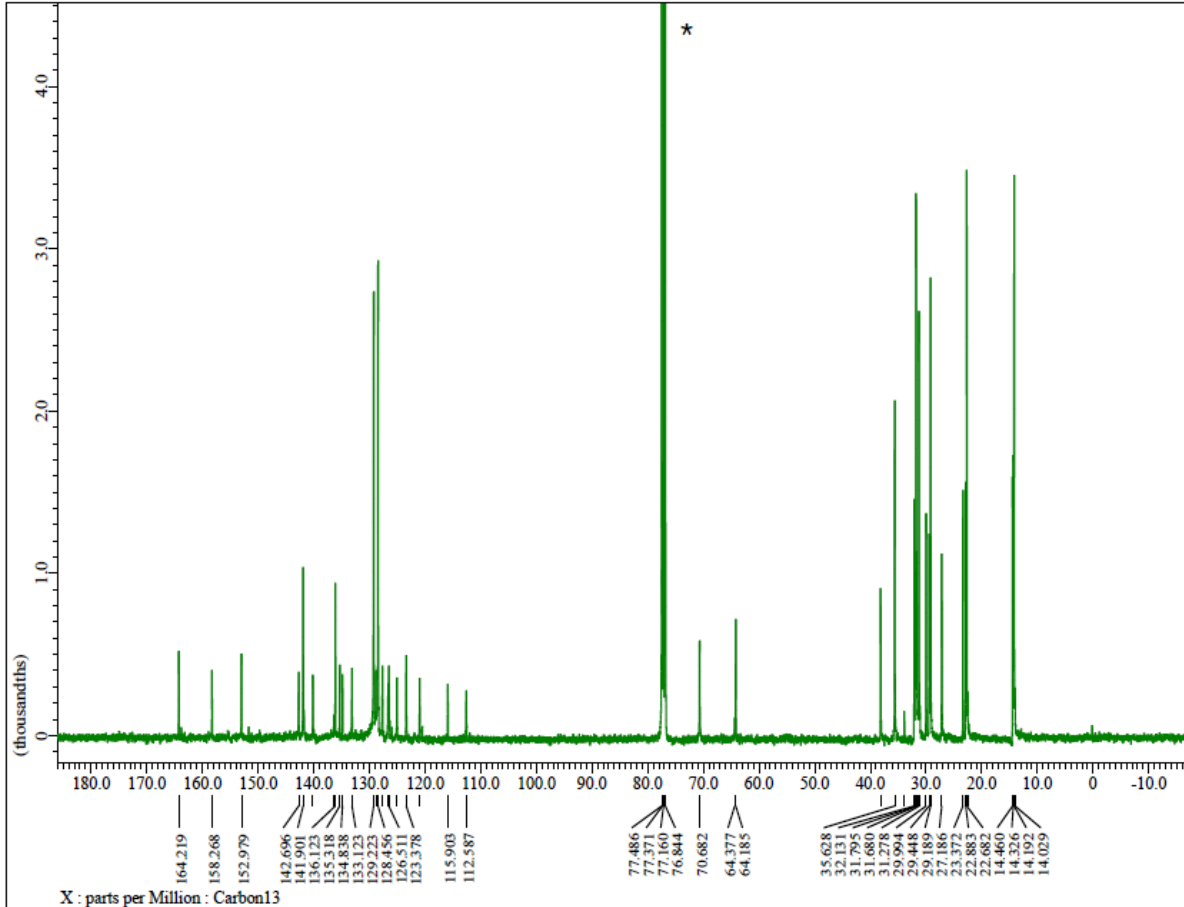
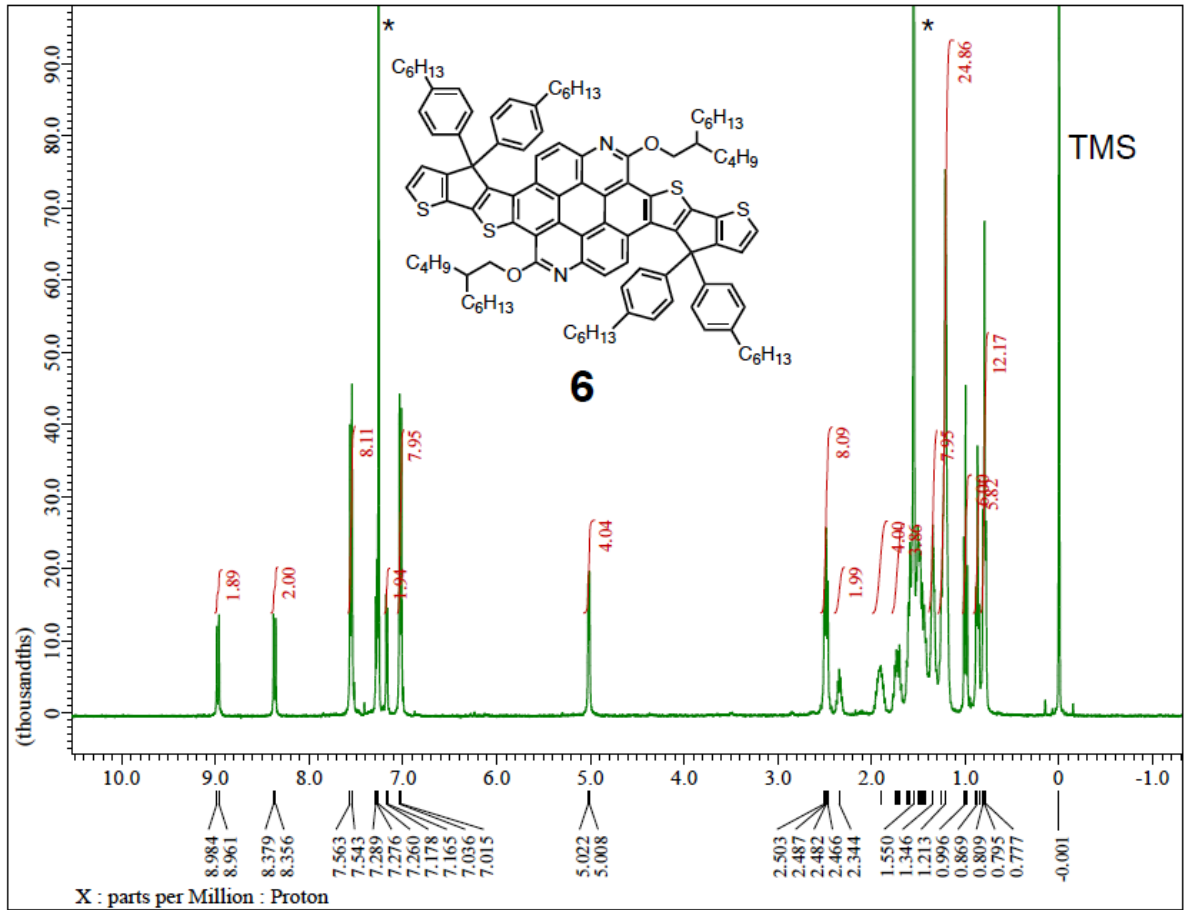
(a)



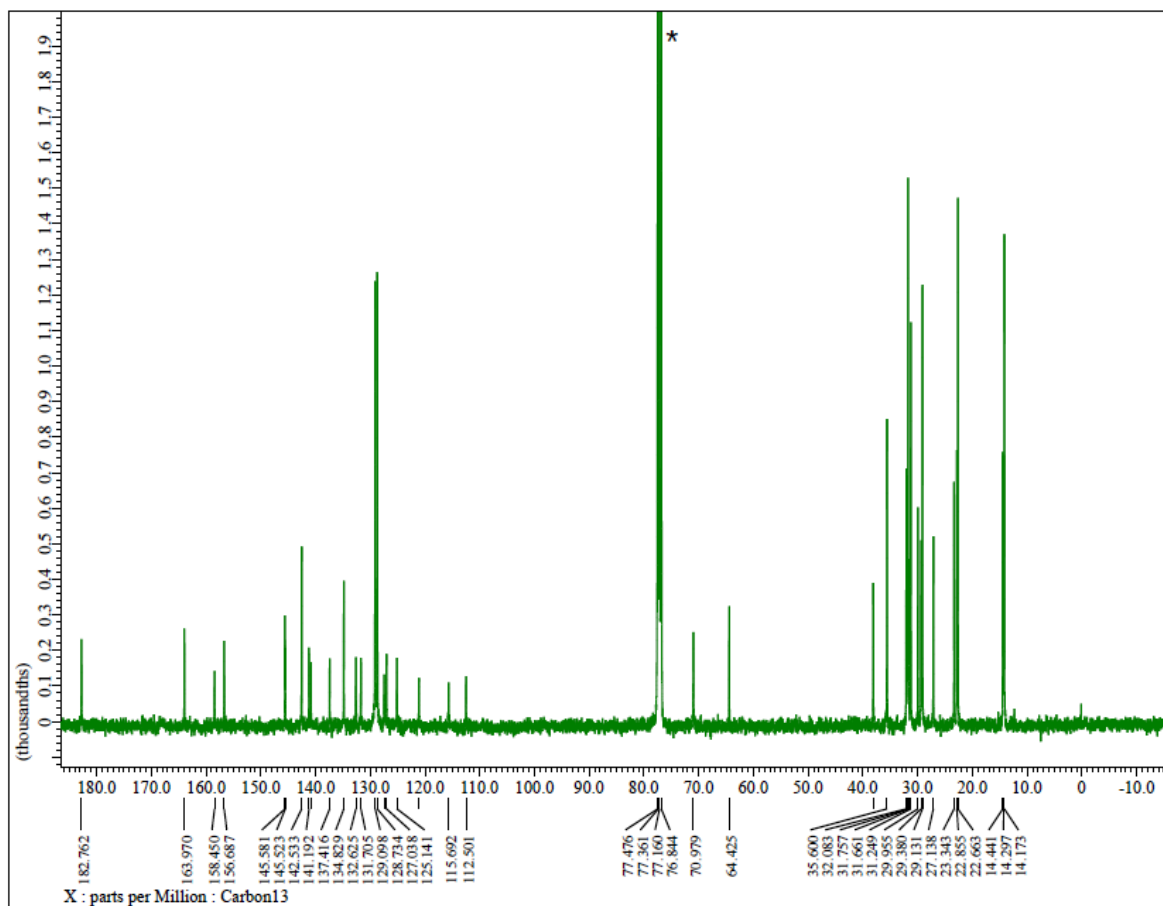
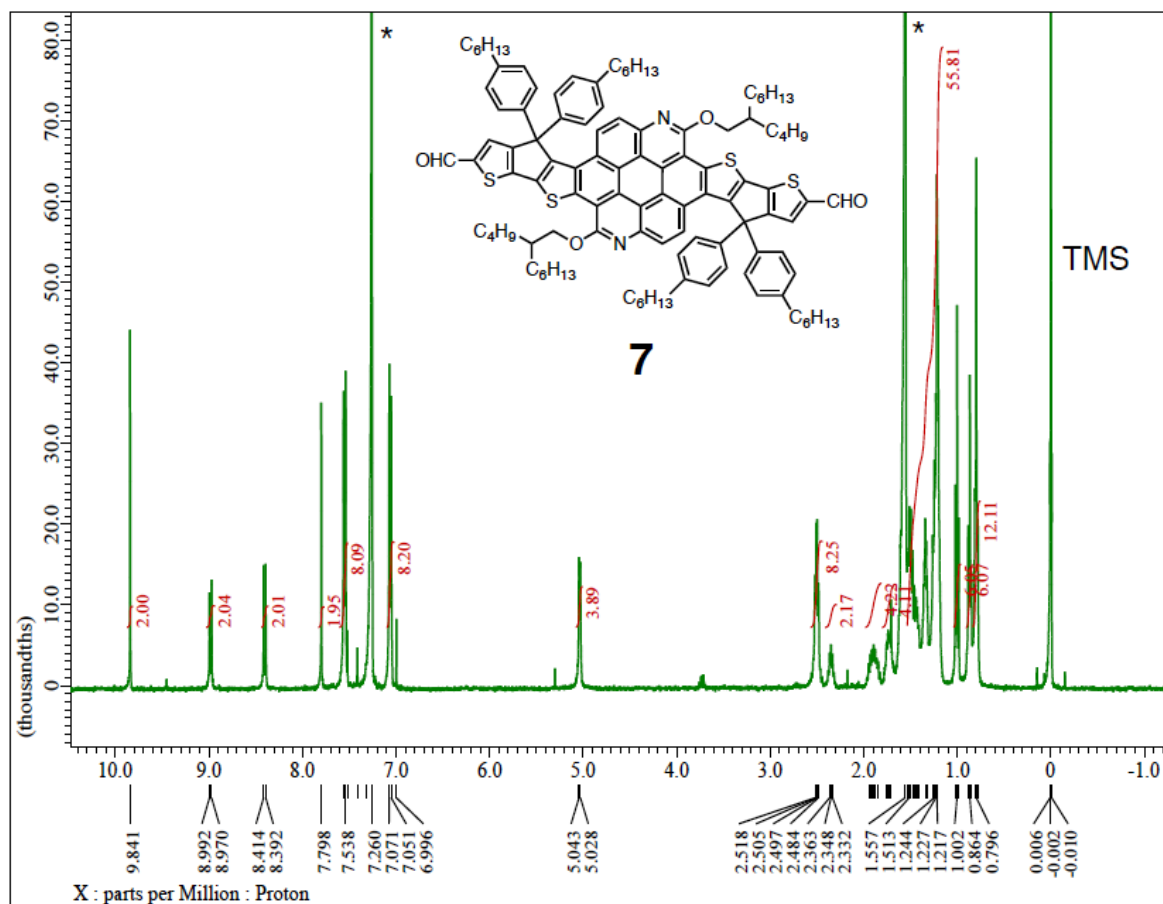
(b)



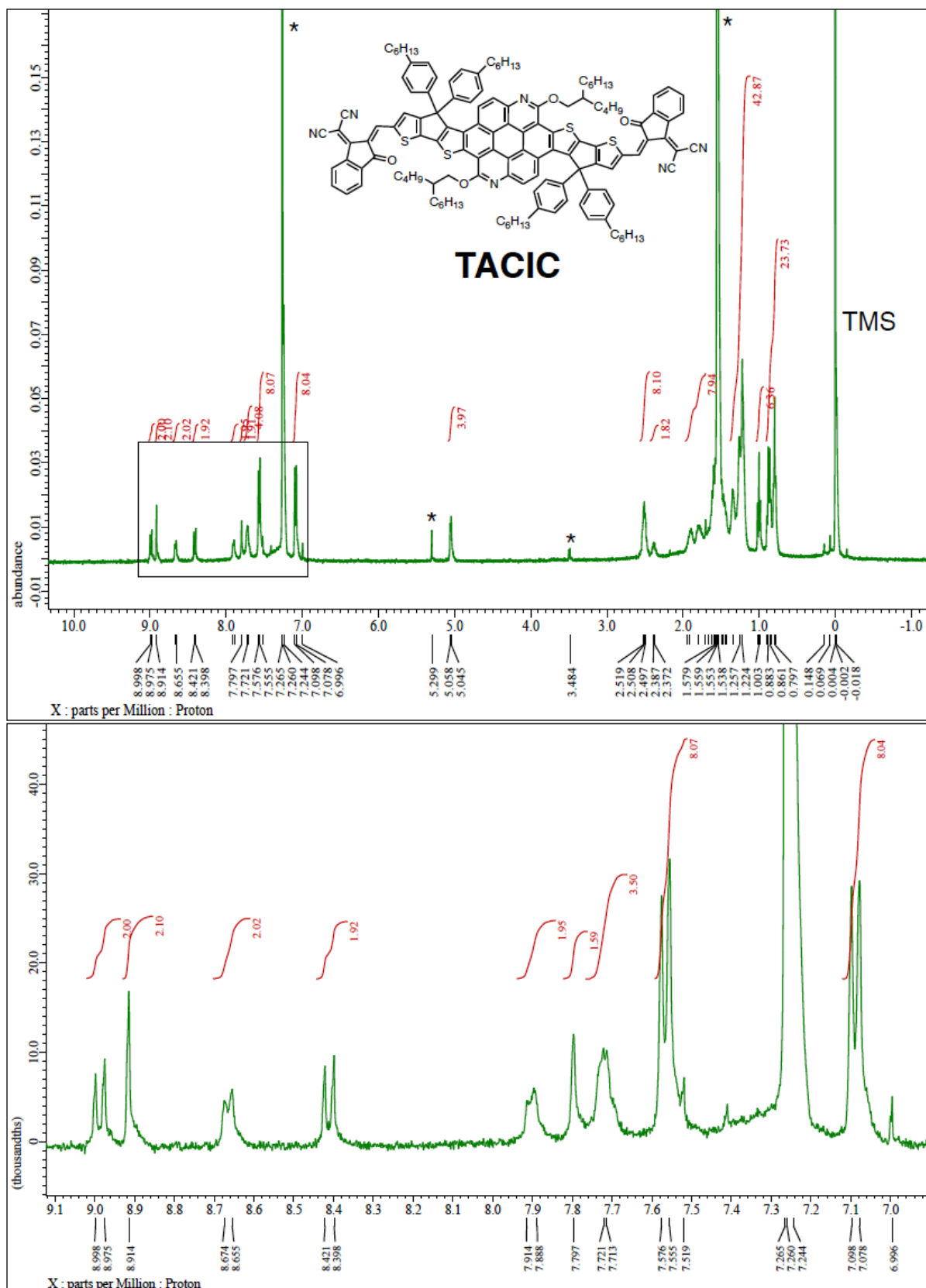
(c)



(d)



(e)



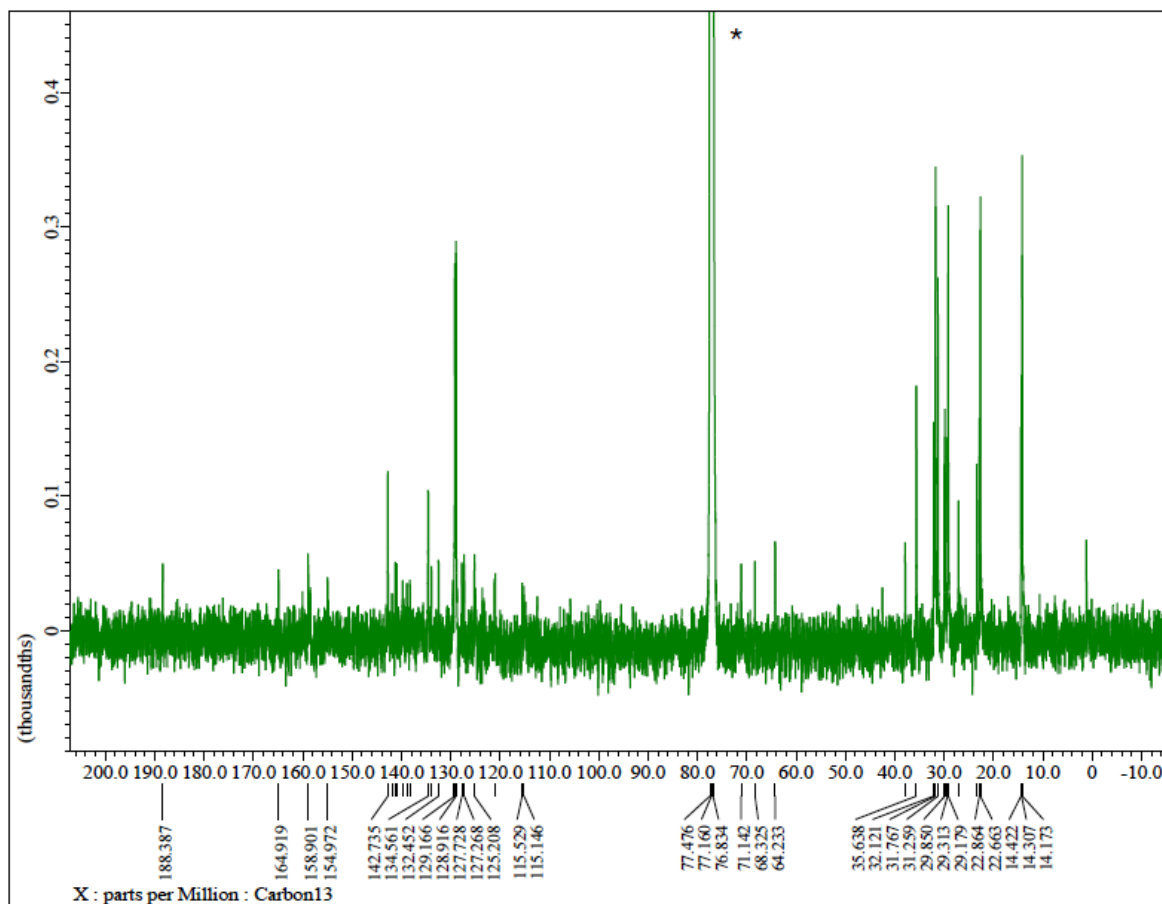


Fig. S1 ^1H (upper) and ^{13}C (lower) NMR spectra of (a) **3**, (b) **4**, (c) **6**, (d) **7**, and (e) TACIC in CDCl_3 . Peaks marked with * arise from residual solvents.

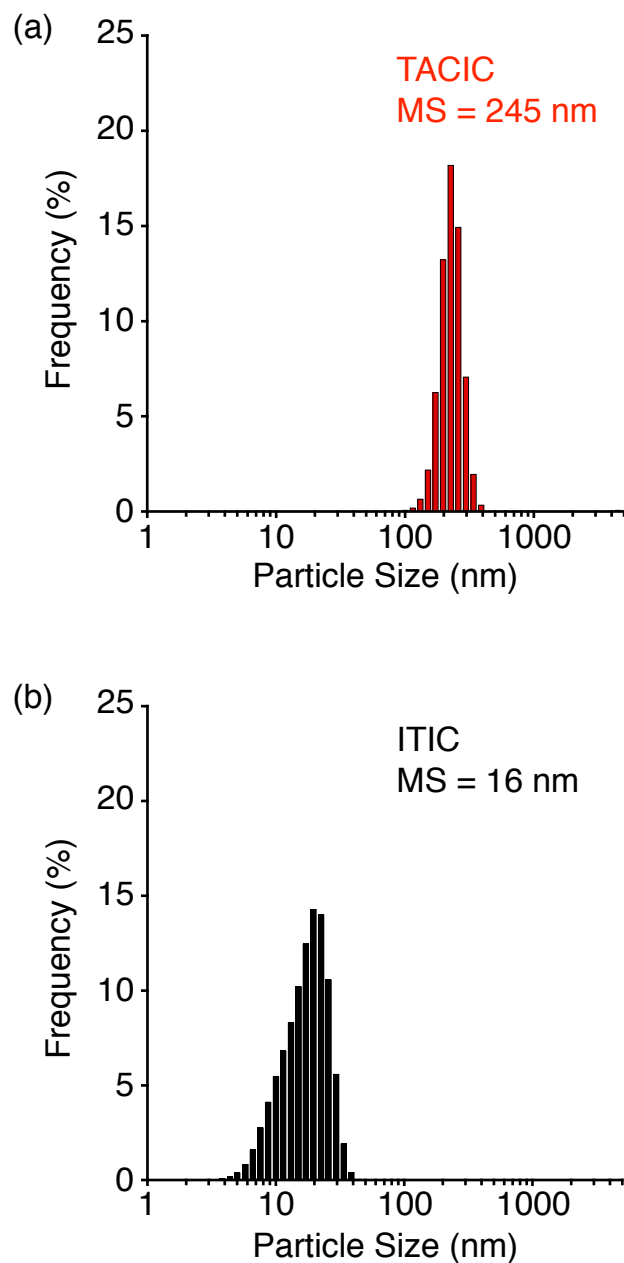


Fig. S2 Particle size distributions of (a) TACIC and (b) ITIC in chloroform at room temperature determined by DLS. Concentration: $[TACIC] = [ITIC] = 6 \text{ mg mL}^{-1}$. Median size (M.S.) values are shown.

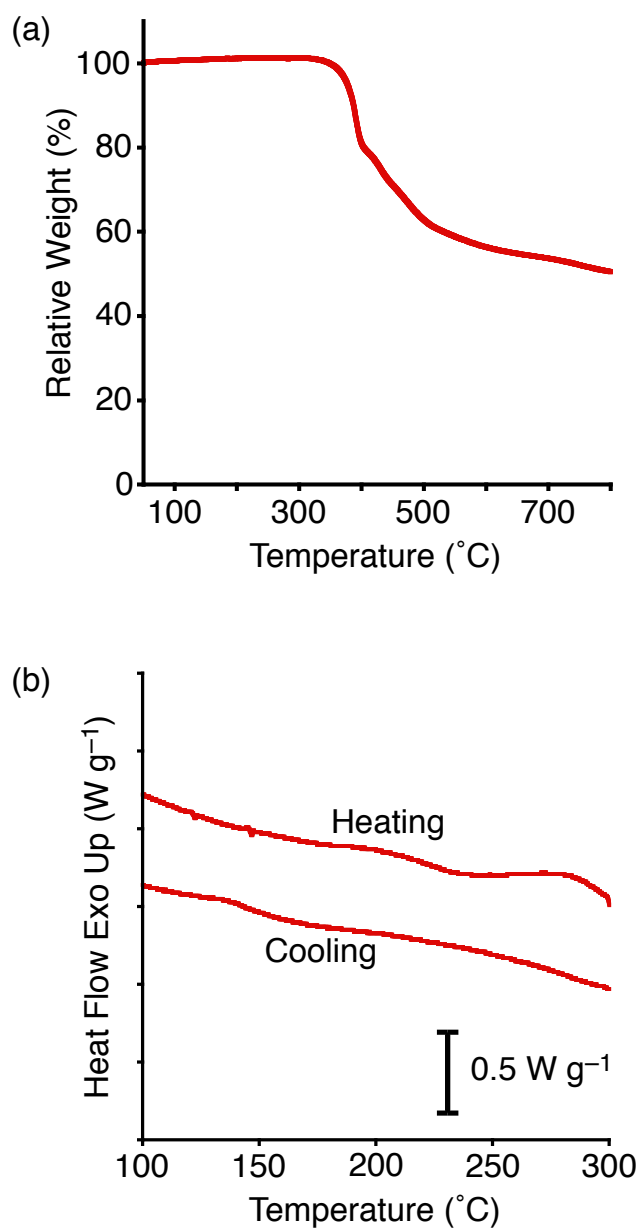


Fig. S3 (a) TGA and (b) DSC curves of TACIC. The analyses were performed under flowing nitrogen at a scan rate of 10 °C min⁻¹. The decomposition temperature (T_d , 5% weight loss) was estimated to be 380 °C in (a).

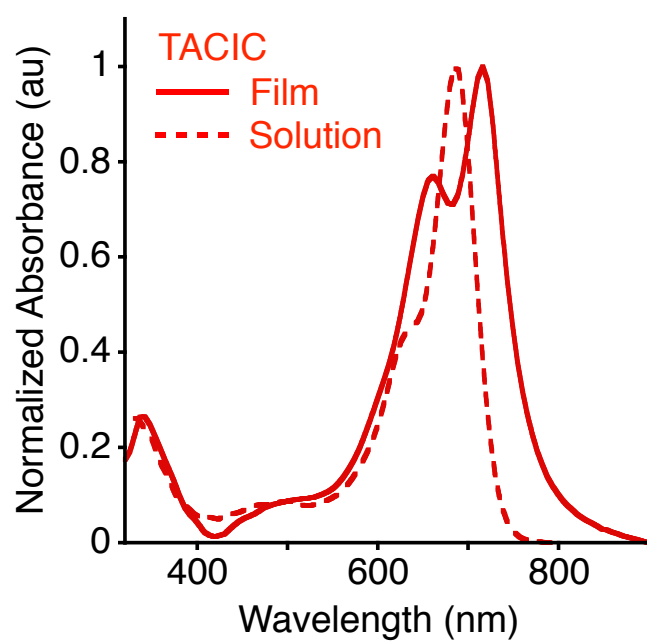


Fig. S4 UV-vis-NIR absorption spectra of TACIC in film state and in chloroform.

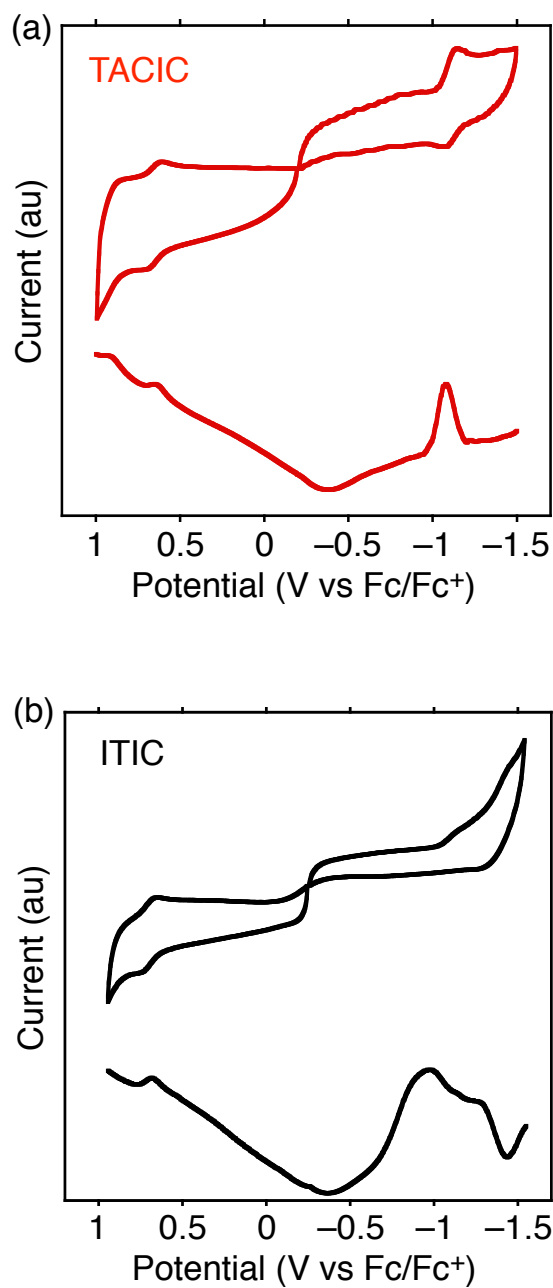


Fig. S5 Cyclic voltammograms (CVs) and differential pulse voltammograms (DPVs) of (a) TACIC and (b) ITIC in dichloromethane containing 0.1 M Bu₄NPF₆. Sweep rate: 0.1 V s⁻¹; reference electrode, Ag/AgNO₃ (0.01 M AgNO₃, 0.09 M Bu₄PF₆ in acetonitrile).

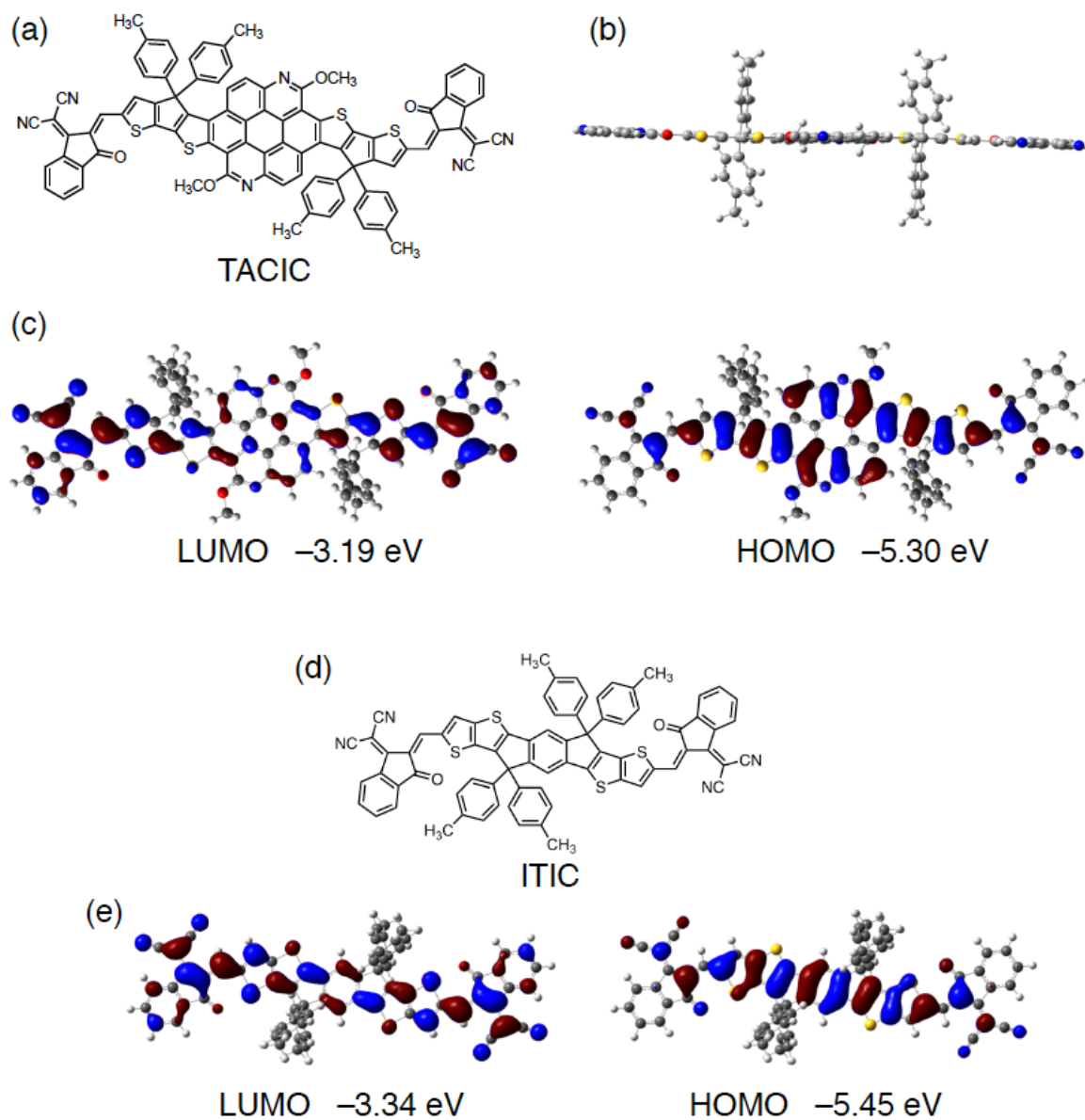


Fig. S6 (a) Structure of TACIC. Alkyl chains were simplified to methyl groups. (b) Optimized structure (side view) and (c) contour plots of frontier molecular orbitals simulated by the DFT calculations using B3LYP/6-31G(d) model for the simplified TACIC. The energy levels are also shown. (d) Structure of ITIC. Alkyl chains were simplified to methyl groups. (e) Contour plots of frontier molecular orbitals for the simplified ITIC.

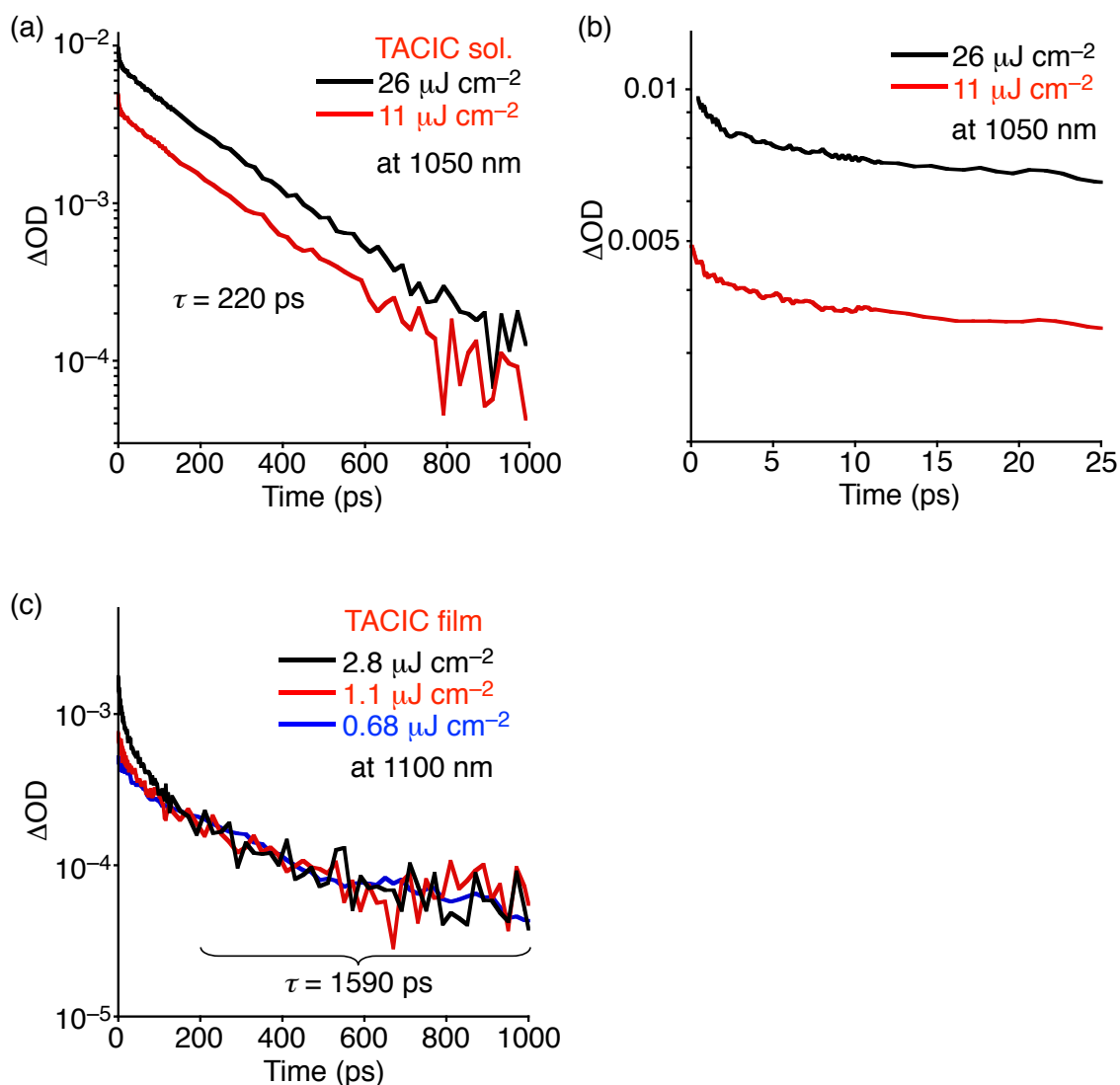


Fig. S7 Transient absorption profiles of singlet excited states of (a,b) TACIC in chloroform measured at a wavelength (λ_{obs}) of 1050 nm and in time ranges of (a) 0–1000 ps and (b) 0–25 ps and (c) TACIC film at $\lambda_{\text{obs}} = 1100$ nm and in a time range of 0–1000 ps. The excitation intensity ranged from 11 to 26 $\mu\text{J cm}^{-2}$ in (a),(b) and from 0.68 to 2.8 $\mu\text{J cm}^{-2}$ in (c). The excitation wavelengths were 650 nm in (a),(b) and 700 nm in (c). In (c), ΔOD values with the excitation intensities of 1.1 and 0.68 $\mu\text{J cm}^{-2}$ are normalized to that with the excitation intensity of 2.8 $\mu\text{J cm}^{-2}$ at 180 ps.

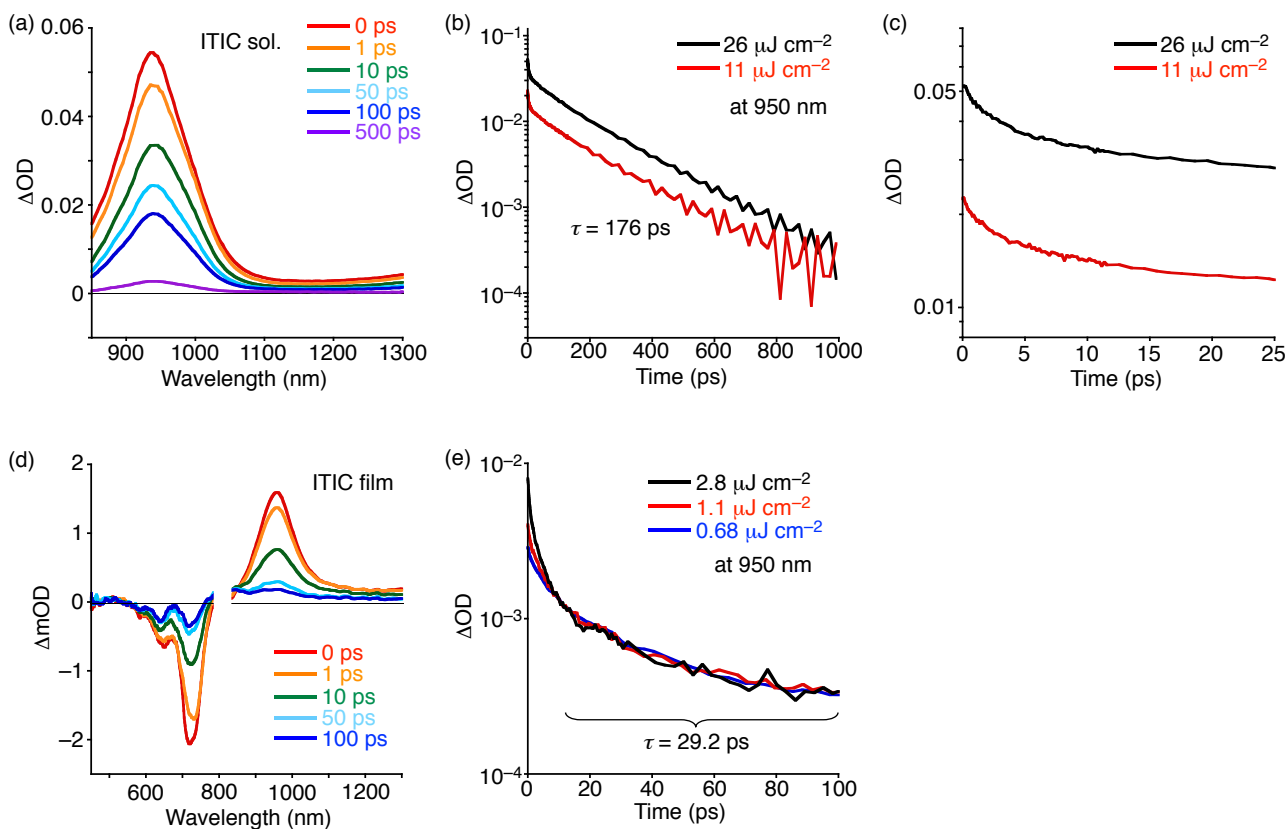


Fig. S8 Transient absorption spectra of (a) ITIC in chloroform measured at 0–500 ps and (d) ITIC film measured at 0–100 ps. The excitation wavelength and intensity were 650 nm and $26 \mu\text{J cm}^{-2}$ in (a) and 700 nm and $0.68 \mu\text{J cm}^{-2}$ in (d). Transient absorption profiles of singlet excited states of ITIC in chloroform at $\lambda_{\text{obs}} = 950$ nm and in time ranges of (b) 0–1000 ps and (c) 0–25 ps and (e) ITIC film at $\lambda_{\text{obs}} = 950$ nm. The excitation intensity ranged from 11 to $26 \mu\text{J cm}^{-2}$ in (b),(c) and from 0.68 to $2.8 \mu\text{J cm}^{-2}$ in (e). In (e), ΔOD values with the excitation intensities of 1.1 and $0.68 \mu\text{J cm}^{-2}$ are normalized to that with the excitation intensity of $2.8 \mu\text{J cm}^{-2}$ at 10 ps.

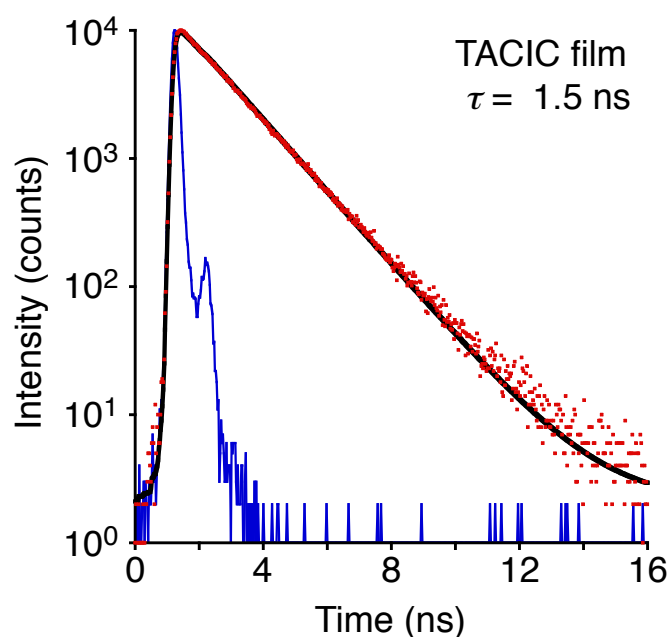


Fig. S9 Nanosecond fluorescence decay (red), decay fitting (black line), and instrumental response function (blue line) of TACIC film measured by TCSPC technique. The excitation and emission wavelengths were 636 and 781 nm. The fluorescence lifetime was calculated to be 1.5 ns. Nanosecond fluorescence decays of TACIC and ITIC in chloroform solution and the ITIC film were also measured by TCSPC technique, but the fluorescence lifetimes could not be estimated due to the shorter lifetimes than the time resolution of the instrument (ca. 200 ps). These results are consistent with the TA spectra (Figs. 3, S7, and S8).

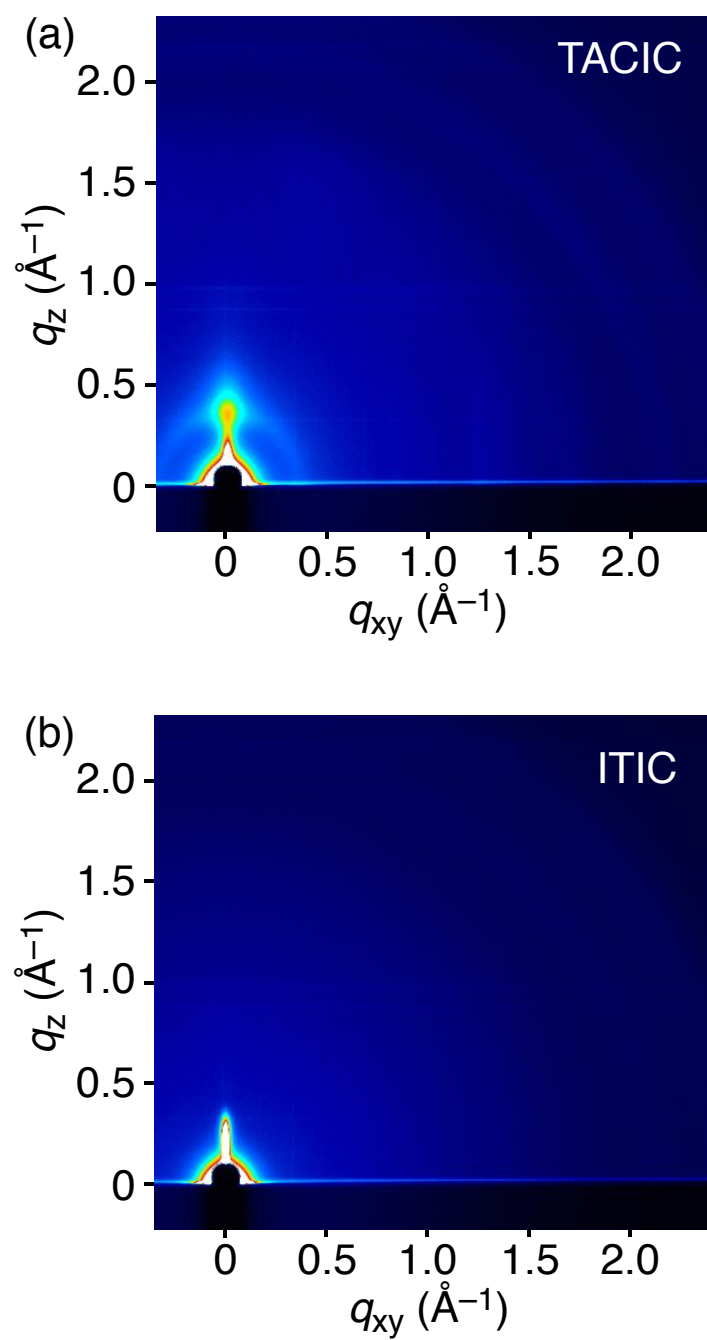


Fig. S10 Two dimensional GIWAXS plots of (a) TACIC and (b) ITIC films on ITO/ZnO substrates.

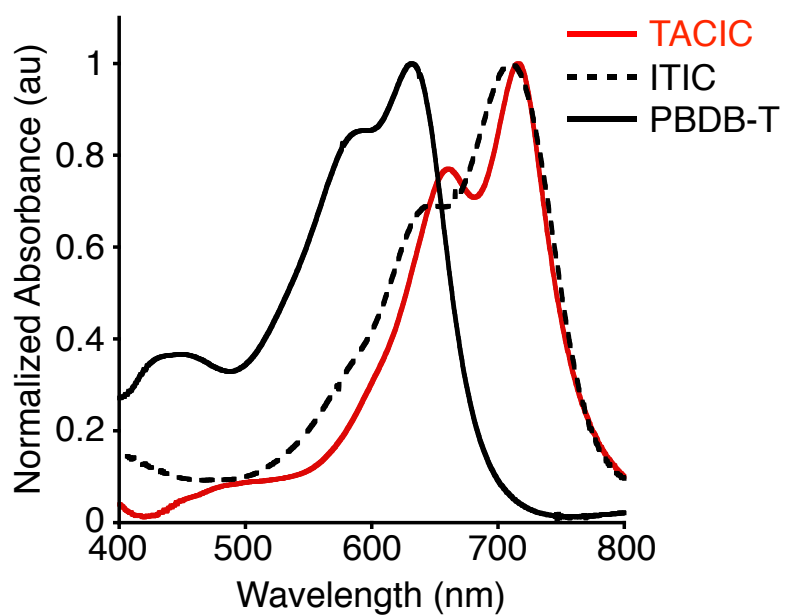


Fig. S11 Normalized UV-vis-NIR absorption spectra of films of TACIC, ITIC, and PBDB-T.

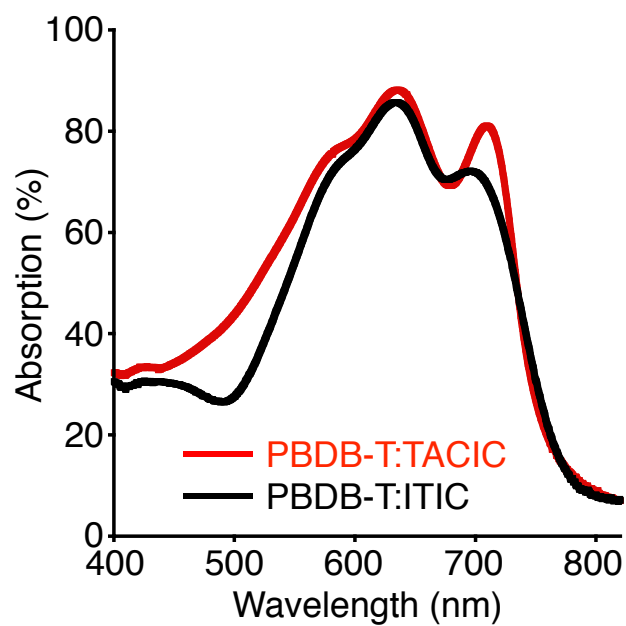


Fig. S12 UV-vis-NIR absorption spectra of the blend films of PBDB-T with TACIC and ITIC on ITO/ZnO substrates. Note here that the total absorption of the ITO/ZnO/PBDB-T:NFA/MoO₃/Ag devices are higher than the values in this figure due to the reflection from the Ag electrode.

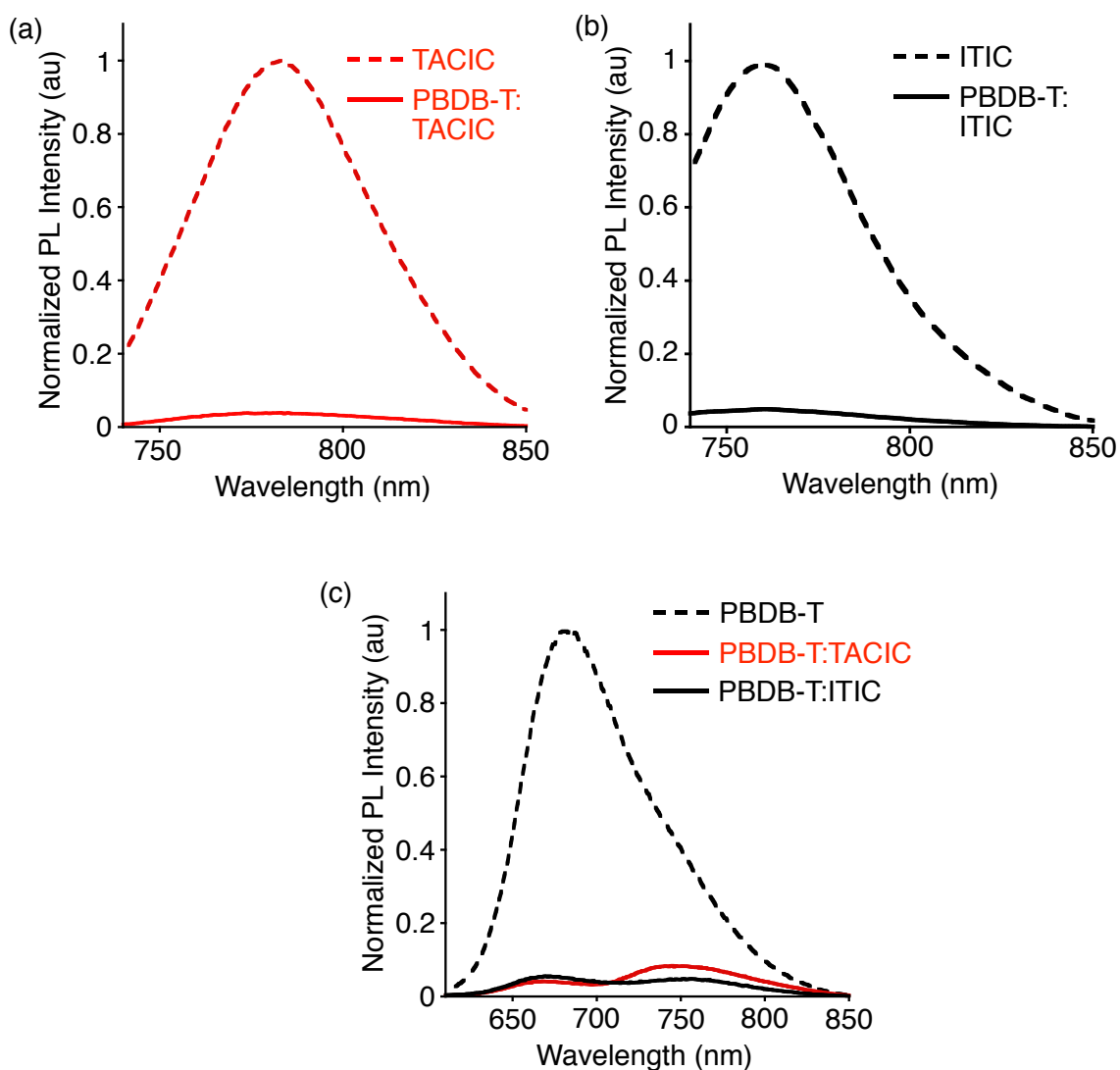


Fig. S13 (a,b) Photoluminescence spectra of (a) TACIC single component film (red dotted) and PBDB-T:TACIC (red solid) and (b) ITIC single component film (black dotted) and PBDB-T:ITIC (black solid). The samples were excited at 710 nm, where the NFAs were predominantly excited. The emission intensities are normalized by that of the acceptor single component film considering the difference in the absorbances of the PBDB-T:NFA films at the excitation wavelength. (c) Photoluminescence spectra of PBDB-T single component film (black dotted) and blend films of PBDB-T with TACIC (red solid) and ITIC (black solid). The excitation wavelength was 520 nm where PBDB-T was predominantly excited. The emission intensities are normalized by that of the PBDB-T single component film considering the difference in the absorbances of the PBDB-T:NFA films at the excitation wavelength.

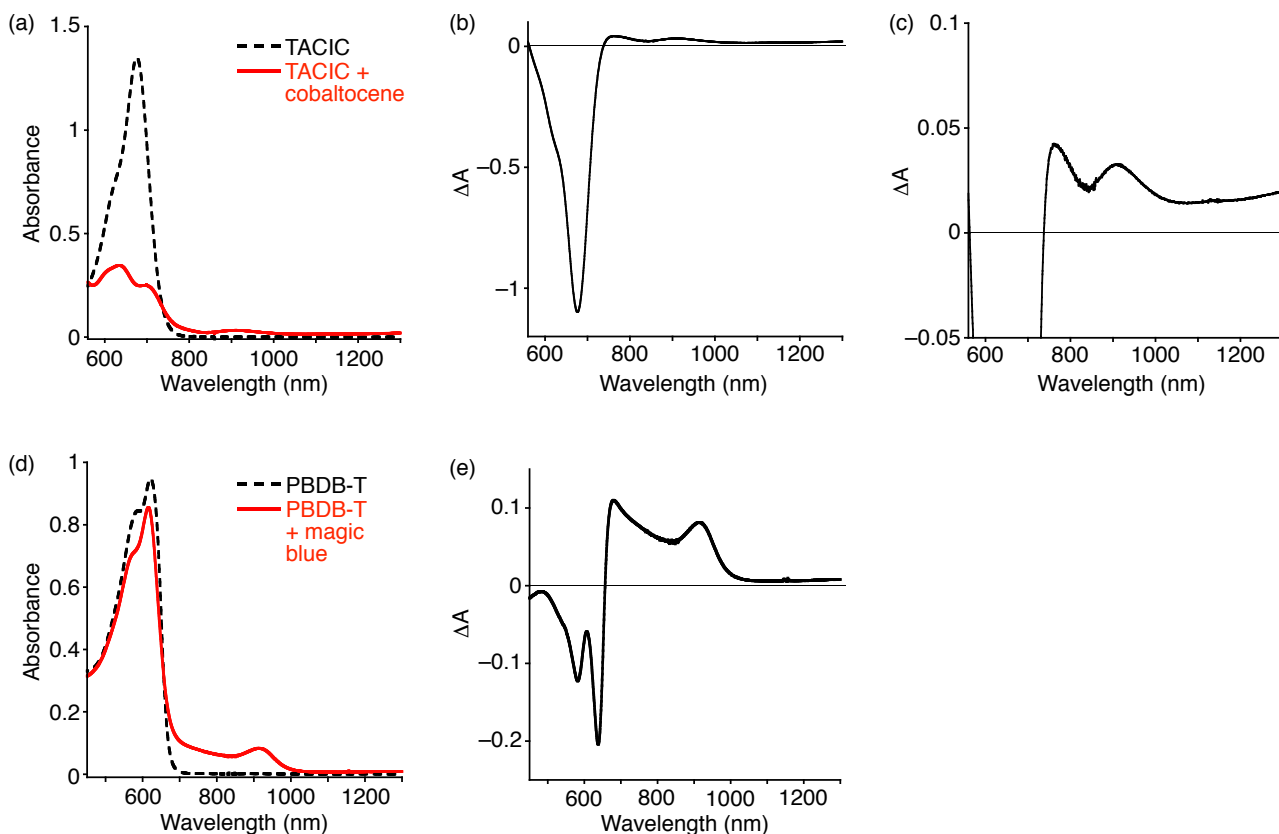


Fig. S14 (a) Vis–NIR absorption spectra of TACIC (1.0×10^{-5} M) (black dotted line) and TACIC (1.0×10^{-8} M) with cobaltocene (1.0×10^{-8} M) as a reductant (red solid line) in CHCl₃. (b),(c) Differential spectrum ((red solid line) – (black dotted line) in (a)) corresponding to the absorption of TACIC anion. (d) Vis–NIR absorption spectra of PBDB-T (1.4×10^{-8} M by repeating unit) (black dotted line) and PBDB-T (1.4×10^{-8} M by repeating unit) with magic blue (3.2×10^{-9} M) as an oxidant (red solid line) in CHCl₃. (e) Differential spectrum ((red solid line) – (black dotted line) in (d)) corresponding to the absorption of PBDB-T hole polaron.

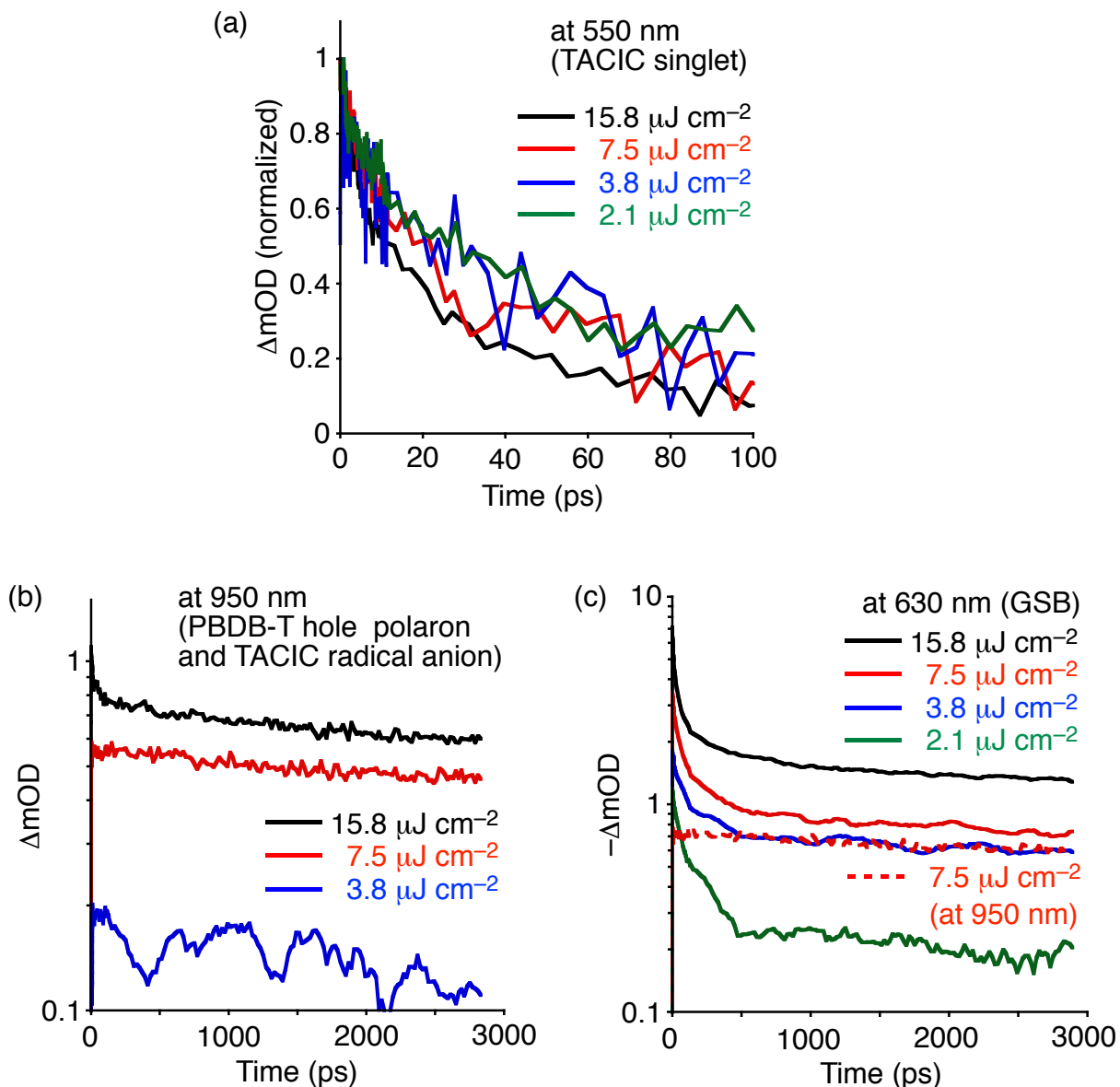


Fig. S15 Transient absorption profiles of (a) singlet excited state of TACIC at 550 nm, (b) PBDB-T hole polaron and TACIC radical anion at 950 nm, and (c) ground state bleaching (GSB) of PBDB-T and TACIC at 630 nm in the PBDB-T:TACIC blend film. The excitation wavelength was 700 nm, and the excitation intensity ranged from 2.1 to 15.8 $\mu\text{J cm}^{-2}$.

The lifetime of S_1 of TACIC in PBDB-T:TACIC was determined to be ca. 60 ps with the excitation intensity of $<7.5 \mu\text{J cm}^{-2}$. This value agrees well with the TACIC S_1 lifetime in TACIC single-component film (1590 ps, Fig. S7c) and photoluminescence quenching efficiency (96%, Fig. S13a) of TACIC in PBDB-T:TACIC.

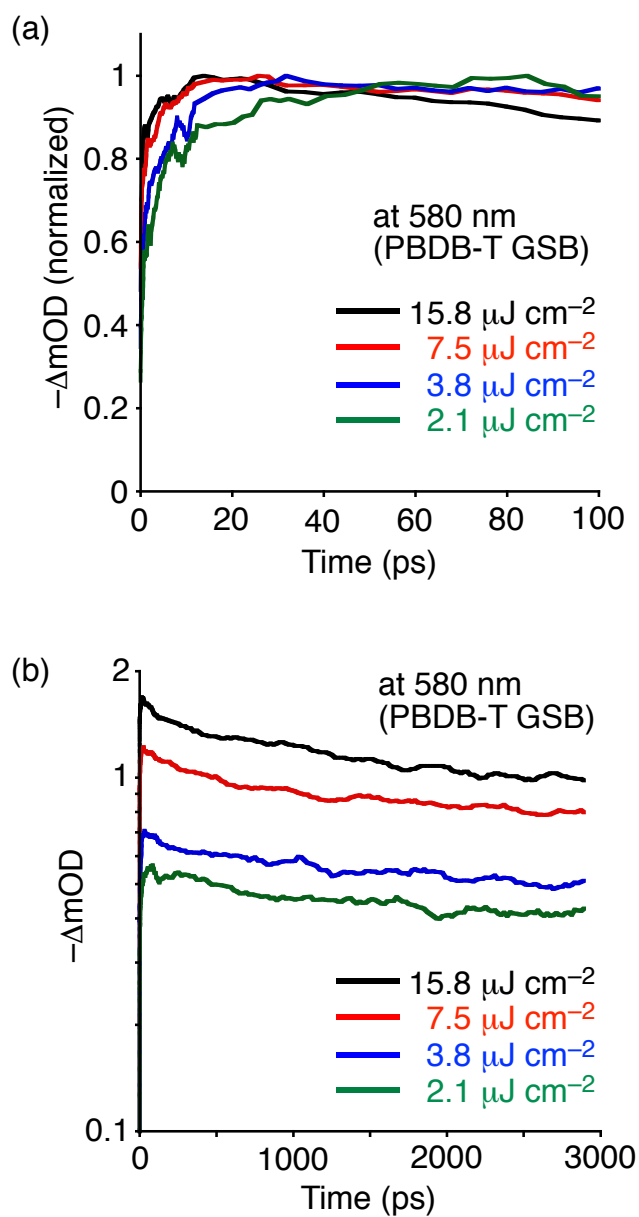


Fig. S16 Transient absorption profile of ground state bleaching (GSB) of PBDB-T in the PBDB-T:ITIC blend film at 580 nm in time ranges of (a) 0–100 ps and (b) 0–3000 ps. The excitation wavelength was 700 nm and the excitation intensity ranged from 2.1 to 15.8 $\mu\text{J cm}^{-2}$.

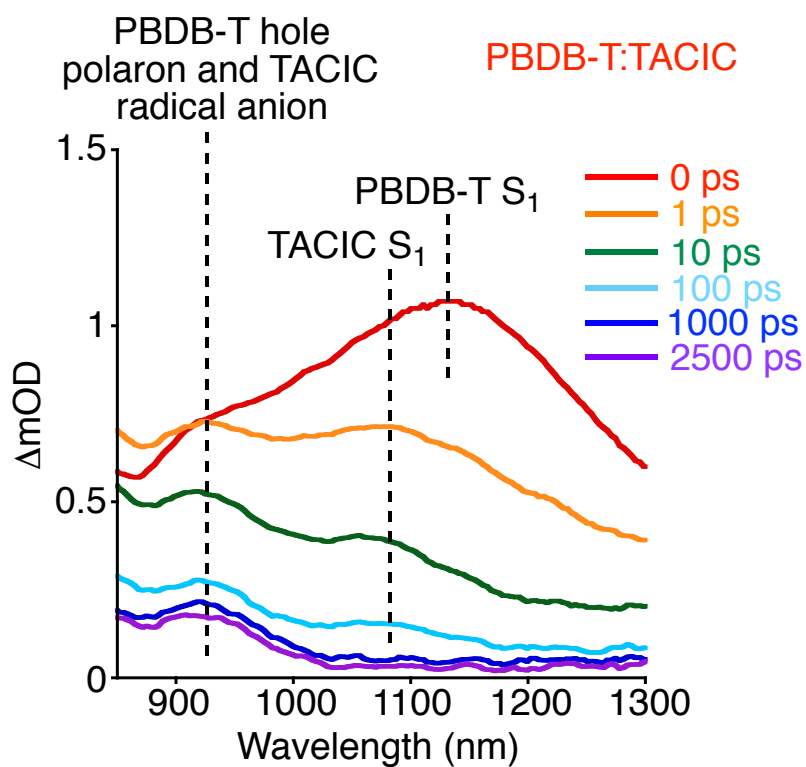


Fig. S17 Transient absorption spectra of the PBDB-T:TACIC blend film measured at 0–2500 ps. The excitation wavelength and intensity were 580 nm and $1.3 \mu\text{J cm}^{-2}$.

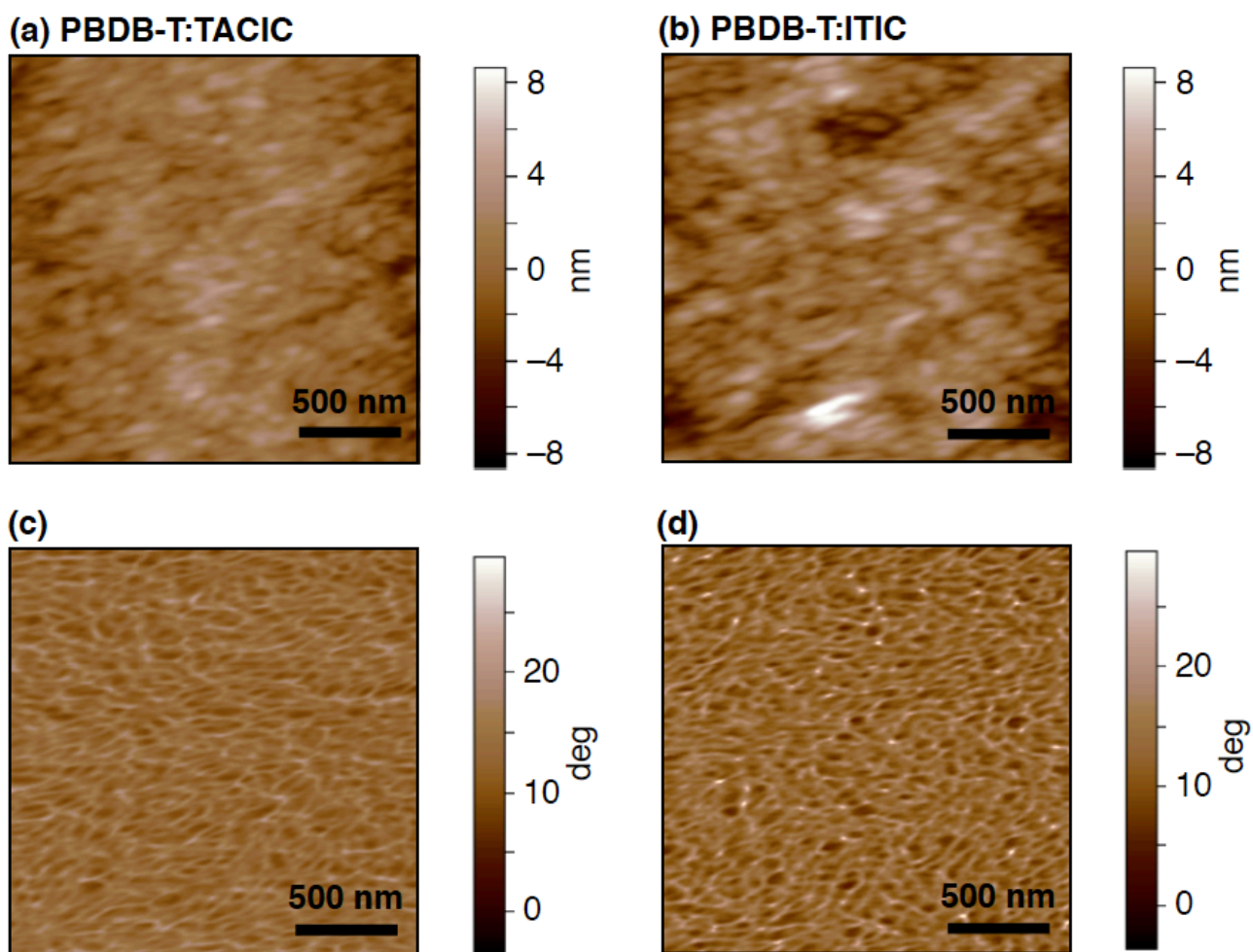


Fig. S18 AFM topography images of (a) PBDB-T:TACIC and (b) PBDB-T:ITIC and phase images of (c) PBDB-T:TACIC and (d) PBDB-T:ITIC on ITO/ZnO substrates. The morphologies are similar to each other and the root-mean-square (rms) surface roughnesses are comparable (1.4 and 1.9 nm in (a) and (b), respectively).

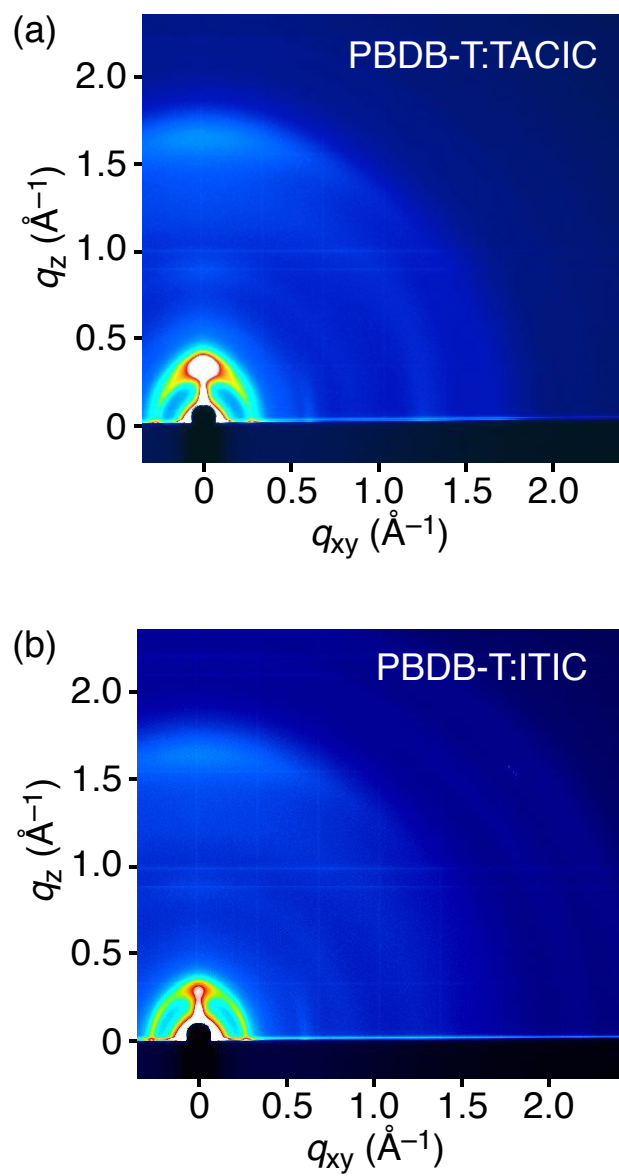


Fig. S19 Two dimensional GIWAXS plots of (a) PBDB-T:TACIC and (b) PBDB-T:ITIC on ITO/ZnO substrates.

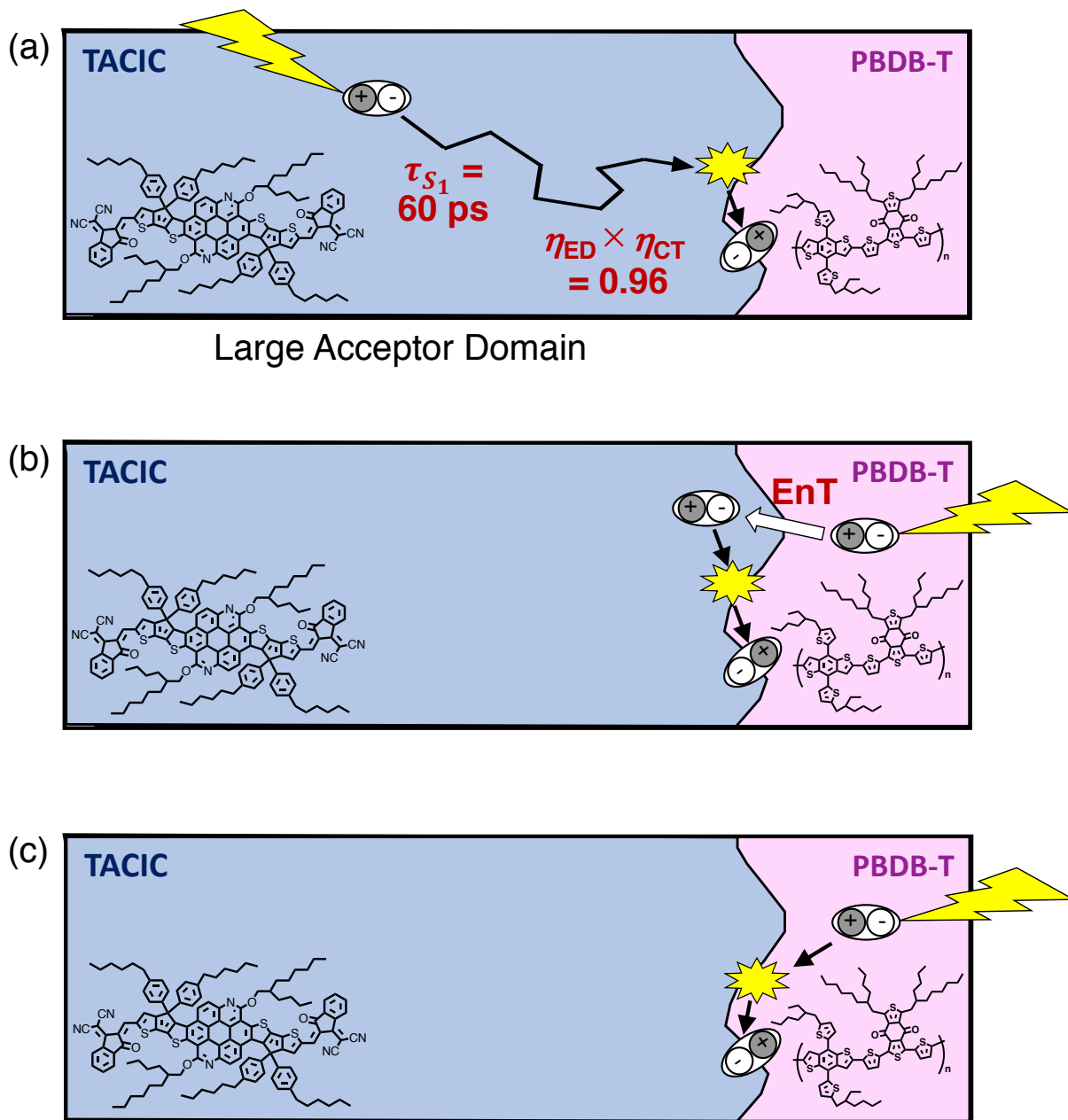


Fig. S20 Schematic view of photocurrent generation mechanisms in the PBDB-T:TACIC blend film. (a) LH, ED, and CT starting from TACIC. (b) LH, EnT, ED, and CT starting from PBDB-T. (c) LH, ED, and CT starting from PBDB-T. It should be emphasized that the process (a) is extremely efficient (the overall efficiency of ED and CT is 96%) and the process (b) is unusual, whereas the process (c) is conventional.

References

- [S1] M. J. Frisch, G. W. Trucks, H. B. Schlegel, G. E. Scuseria, M. A. Robb, J. R. Cheeseman, G. Scalmani, V. Barone, B. Mennucci, G. A. Petersson, H. Nakatsuji, M. Caricato, X. Li, H. P. Hratchian, A. F. Izmaylov, J. Bloino, G. Zheng, J. L. Sonnenberg, M. Hada, M. Ehara, K. Toyota, R. Fukuda, J. Hasegawa, M. Ishida, T. Nakajima, Y. Honda, O. Kitao, H. Nakai, T. Vreven, J. A. Montgomery, Jr., J. E. Peralta, F. Ogliaro, M. Bearpark, J. J. Heyd, E. Brothers, K. N. Kudin, V. N. Staroverov, R. Kobayashi, J. Normand, K. Raghavachari, A. Rendell, J. C. Burant, S. S. Iyengar, J. Tomasi, M. Cossi, N. Rega, J. M. Millam, M. Klene, J. E. Knox, J. B. Cross, V. Bakken, C. Adamo, J. Jaramillo, R. Gomperts, R. E. Stratmann, O. Yazyev, A. J. Austin, R. Cammi, C. Pomelli, J. W. Ochterski, R. L. Martin, K. Morokuma, V. G. Zakrzewski, G. A. Voth, P. Salvador, J. J. Dannenberg, S. Dapprich, A. D. Daniels, Ö. Farkas, J. B. Foresman, J. V. Ortiz, J. Cioslowski and D. J. Fox, *Gaussian 09*, Gaussian, Inc., Wallingford CT, 2009.
- [S2] B. He, J. Dai, D. Zherebetsky, T. L. Chen, B. A. Zhang, S. J. Teat, Q. Zhang, L. Wang and Y. Liu, *Chem. Sci.*, 2015, **6**, 3180.
- [S3] Y. Wang, H. Guo, S. Ling, I. Arrechea-Marcos, Y. Wang, J. T. L. Navarrete, R. P. Ortiz and X. Guo, *Angew. Chem. Int. Ed.*, 2017, **56**, 9924.
- [S4] J. M. Tobin, J. Liu, H. Hayes, M. Demleitner, D. Ellis, V. Arrighi, Z. Xu and F. Vilela, *Polym. Chem.*, 2016, **7**, 6662.
- [S5] Y. Cui, H. Ren, J. Yu, Z. Wang and G. Qian, *Dyes Pigm.*, 2009, **81**, 53.
- [S6] B. He, A. B. Pun, L. M. Klivansky, A. M. McGough, Y. Ye, J. Zhu, J. Guo, S. J. Teat and Y. Liu, *Chem. Mater.*, 2014, **26**, 3920.
- [S7] (a) N. D. Eastham, J. L. Logsdon, E. F. Manley, T. J. Aldrich, M. J. Leonardi, G. Wang, N. E. Powers-Riggs, R. M. Young, L. X. Chen, M. R. Wasielewski, F. S. Melkonyan, R. P. H. Chang and T. J. Marks, *Adv. Mater.*, 2018, **30**, 1704263; (b) X. Yi, B. Gautam, I. Constantinou, Y. Cheng, Z. Peng, E. Klump, X. Ba, C. H. Y. Ho, C. Dong, S. R. Marder, J. R. Reynolds, S.-W. Tsang, H. Ade and F. So, *Adv. Funct. Mater.*, 2018, **28**, 1802702.
- [S8] (a) B. Kan, J. Zhang, F. Liu, X. Wan, C. Li, X. Ke, Y. Wang, H. Feng, Y. Zhang, G. Long, R. H. Friend, A.A. Bakulin and Y. Chen, *Adv. Mater.*, 2018, **30**, 1704904; (b) O. M. Awartani, B. Gautam, W. Zhao, R. Younts, J. Hou, K. Gundogdu and H. Ade, *J. Mater. Chem. A*, 2018, **6**, 12484; (c) T. R. Hopper, D. Qian, L. Yang, X. Wang, K. Zhou, R. Kumar, W. Ma, C. He, J. Hou, F. Gao and A. A. Bakulin, *Chem. Mater.*, 2019, **31**, 6860.